JGR Biogeosciences

RESEARCH ARTICLE
10.1029/2021JG006568

Quantification of Urban Forest and Grassland Carbon Fluxes Using Field Measurements and a Satellite-Based Model in Washington DC/Baltimore Area

J. B. Winbourne[1,2], I. A. Smith[1], H. Stoynova[1], C. Kohler[3], C. K. Gately[1,4], B. A. Logan[5], J. Reblin[5], A. Reinmann[3,6], D. W. Allen[7], and L. R. Hutyra[1]

[1]Department of Earth and Environment, Boston University, Boston, MA, USA, [2]Department of Earth, Environment, and Atmospheric Sciences, University of Massachusetts Lowell, Lowell, MA, USA, [3]City University of New York Advanced Science Research Center, Environmental Sciences Initiative, New York, NY, USA, [4]Metropolitan Area Planning Council, Boston, MA, USA, [5]Biology Department, Bowdoin College, Brunswick, ME, USA, [6]Department of Geography and Environmental Science, Hunter College, New York, NY, USA, [7]National Institute of Standards and Technology, Gaithersburg, MD, USA

Abstract Cities are taking the lead on climate change mitigation with ambitious goals to reduce carbon dioxide (CO_2) emissions. The implementation of effective mitigation policies will require accurate measurements to guide policy decisions and monitor their efficacy. Here, we present a comprehensive CO_2 inventory of an urban temperate forest and unmanaged grassland using field observations. We estimate the annual storage of CO_2 by vegetation and soils and place our biogenic flux estimates in the context of local fossil fuel (FF) emissions to determine when, where, and by how much biogenic fluxes alter net CO_2 flux dynamics. We compare our hourly estimates of biogenic fluxes in the forest site to modeled estimates using a modified version of Urban-Vegetation Photosynthesis and Respiration Model (Urban-VPRM) in Washington DC/Baltimore area presenting the first urban evaluation of this model. We estimate that vegetation results in a net biogenic uptake of -2.62 ± 1.9 Mg C ha^{-1} yr^{-1} in the forest site. FF emissions, however, drive patterns in the net flux resulting in the region being a net source of CO_2 on daily and annual timescales. In the summer afternoons, however, the net flux is dominated by the uptake of CO_2 by vegetation. The Urban-VPRM closely approximates hourly forest inventory based estimates of gross ecosystem exchange but overestimates ecosystem respiration in the dormant season by 40%. Our study highlights the importance of including seasonal dynamics in biogenic CO_2 fluxes when planning and testing the efficacy of CO_2 emission reduction polices and development of monitoring programs.

Plain Language Summary The quantification of biogenic carbon dioxide (CO_2) fluxes in cities is important to developing, reporting, and testing the efficacy of greenhouse gas emission reduction policies. Yet, to date there is a lack of detailed CO_2 flux inventories conducted in urban ecosystems which is hindering our abilities to advance and evaluate urban carbon cycling models. Our study characterizes how unique features of urbanization influence carbon cycling dynamics in a temperate forest and grassland and provides a critical evaluation of a model for estimating biogenic fluxes of CO_2. We identify key areas of needed model development and identify the seasonal and temporal significance of biogenic fluxes relative to total CO_2 fluxes (biogenic + anthropogenic sources) in our study area.

Key Points:

- In urban landscapes, the biogenic carbon dioxide (CO_2) fluxes from forest patches and grassland areas vary at fine temporal and spatial scales
- The Urban-Vegetation Photosynthesis and Respiration Model closely approximated temporal trends in gross ecosystem exchange but overestimated ecosystem respiration in the wintertime
- Fossil fuel emissions drive patterns in the net flux of CO_2 except in summer afternoons when biogenic fluxes dominate

Supporting Information:

Supporting Information may be found in the online version of this article.

Correspondence to:

J. B. Winbourne,
joywinbourne@gmail.com

Citation:

Winbourne, J. B., Smith, I. A., Stoynova, H., Kohler, C., Gately, C. K., Logan, B. A., et al. (2022). Quantification of urban forest and grassland carbon fluxes using field measurements and a satellite-based model in Washington DC/Baltimore area. *Journal of Geophysical Research: Biogeosciences*, *127*, e2021JG006568. https://doi.org/10.1029/2021JG006568

Received 2 AUG 2021
Accepted 15 DEC 2021

Author Contributions:

Conceptualization: J. B. Winbourne, A. Reinmann, L. R. Hutyra
Data curation: J. B. Winbourne, I. A. Smith, H. Stoynova, C. Kohler
Formal analysis: J. B. Winbourne, I. A. Smith
Funding acquisition: B. A. Logan, A. Reinmann, L. R. Hutyra
Investigation: J. B. Winbourne, I. A. Smith, H. Stoynova, C. Kohler, B. A. Logan, J. Reblin, A. Reinmann
Methodology: J. B. Winbourne, I. A. Smith, H. Stoynova, A. Reinmann, L. R. Hutyra
Project Administration: L. R. Hutyra
Software: J. B. Winbourne, I. A. Smith

1. Introduction

Urban biological carbon dioxide (CO_2) sources and sinks strongly influence atmospheric concentrations of CO_2 both globally and locally (Hutyra et al., 2014; Sargent et al., 2018). The abundance of anthropogenic sources of CO_2 in urban areas—70% of global fossil fuel (FF) emissions (Le Quéré et al., 2013; U.S. Energy Information Agency, 2013)—has led to biogenic CO_2 contributions to be assumed as negligible (Chen et al., 2020; Nowak, 1993; Pataki et al., 2009, 2011). Consequently, biogenic sources are largely ignored in bottom-up CO_2 emission inventories (Hutyra et al., 2014; Kennedy et al., 2009; Roest et al., 2020) and remote sensing-based estimates of landscape CO_2 fluxes (Boesch et al., 2011; Churkina, 2008). However, vegetation can comprise a large portion of urban land areas (ranging from 4% to 53%; Lavalle & Martins, 2002; Nowak et al., 2001) and has been found to contribute significantly to urban CO_2 fluxes (Decina et al., 2016; McRae & Graedel, 1979; Miller et al., 2012; Milnar & Ramaswami, 2020; Pataki et al., 2003; Sargent et al., 2018). Globally, efforts are

Supervision: A. Reinmann, D. W. Allen, L. R. Hutyra
Visualization: J. B. Winbourne, I. A. Smith, H. Stoynova, C. K. Gately
Writing – original draft: J. B. Winbourne
Writing – review & editing: J. B. Winbourne, I. A. Smith, B. A. Logan, J. Reblin, A. Reinmann, D. W. Allen, L. R. Hutyra

underway to increase canopy cover in cities to help offset emissions and to cool cities (Fargione et al., 2018; Lamb et al., 2019). While biological uptake of CO_2 in cities has been estimated to offset between 0 and >100% of local FF emissions depending on the locale, season, and hours of the day considered (Lauvaux et al., 2020; M. Zhao et al., 2010; Sargent et al., 2018; Yin et al., 2010), there remains a lack of detailed biological carbon flux measurements to test inventories and model fluxes, hindering our ability to generate accurate modeled estimates of urban CO_2 emissions (Gurney et al., 2005; Hutyra et al., 2014; Kennedy et al., 2012; Lauvaux et al., 2020). As cities across the globe are setting ambitious goals to reduce CO_2 emissions and implement nature-based climate solutions (Fargione et al., 2018; Rosenzweig et al., 2010), CO_2 monitoring systems that include accurate regional modeling tools coupled with evaluation from on-the-ground measurements are needed to guide policies and determine their efficacy (Hsu et al., 2019; W. Zhou et al., 2019).

The challenge in generating empirical estimates of biogenic C fluxes in urban areas is rooted in the variety of sources and sink dynamics that are spatially and temporally variable (Clark et al., 2001). The net CO_2 balance or net ecosystem exchange (NEE) of biogenic CO_2 fluxes is the small difference between large fluxes associated with ecosystem respiration (R_e; year-round fluxes with day/night variations) and photosynthetic C assimilation (growing season and daytime process). While the NEE of biogenic CO_2 is small on an annual basis, the gross ecosystem exchange (GEE) of CO_2 between biosphere and atmosphere is large and varies significantly on diel and seasonal time scales (Hardiman et al., 2017; Hutyra et al., 2014), impacting observed urban atmospheric CO_2 mixing ratios (Sargent et al., 2018). The major components of biogenic R_e are from autotrophic sources (leaf, stem, and root associated respiration) and heterotrophic sources (decomposition of coarse woody debris [CWD] pools and C substrates in the soil). In managed landscapes, the decomposition of imported labile C sources such as compost and mulch can also contribute substantially to heterotrophic respiration (Decina et al., 2016; Hundertmark et al., 2021) The major source of CO_2 uptake is from photosynthetic activity of plants and the storage of this fixed CO_2 in plant biomass and soils which vary in functional type across urban landscapes (Pataki et al., 2006, Figure 1).

Urbanization creates a suite of novel ecosystem conditions that can have important, but poorly constrained impacts on ecosystem CO_2 balance that are not reliably predictable from intact rural systems (Hardiman et al., 2017). Yet, models of CO_2 fluxes that include biological sources are predominantly developed to be used in rural areas. Both bottom-up (Briber et al., 2015; Gough & Elliott, 2012) and top-down (Lauvaux et al., 2020; Pataki et al., 2006; Sargent et al., 2018; Turnbull et al., 2015) approaches for quantifying CO_2 fluxes have demonstrated the enhanced productivity of vegetation in some urban areas. Across many biomes, studies show the potential for large C sequestration rates in cities (Churkina et al., 2010; Jo, 2002; Nowak & Crane, 2002; T. T. Zhao et al., 2012) with enhanced growth rates of urban vegetation (Golubiewski, 2006; Reinmann & Hutyra, 2017; Smith, Dearborn, & Hutyra, 2019). The net productivity per unit plant biomass in cities is stimulated by more optimal plant growth conditions (e.g., temperature, water, light, CO_2, and nutrients) than adjacent rural settings (S. Zhao et al., 2016). For example, urban areas experience elevated ambient air temperatures (the urban heat island effect; Kim, 1992; Oke, 1982) and a lengthening of the urban growing season (Melaas et al., 2016a, 2016b; X. Zhang et al., 2004). Net productivity can be stimulated by elevated ambient CO_2 concentrations (Ainsworth et al., 2012), greater nutrient availability from direct fertilization or indirectly from deposition (Decina et al., 2016; Rao et al., 2014), high light environments (Reinmann et al., 2020; Trlica et al., 2020), and potential for higher water availability from irrigation and leaking infrastructure (Randrup et al., 2001; Stål, 1998). Similarly, urban conditions can elevate soil respiration rates due to the import of labile C sources and use of fertilizers (Decina et al., 2016; Hundertmark et al., 2021; Townsend-Small & Czimczik, 2010).

Conversely, urban conditions can negatively affect net productivity and ecosystem respiration rates. For example, net productivity of vegetation can be decreased through increased pollutant loads (e.g., ozone, heavy metals; Ainsworth et al., 2012; Krupa & Manning, 1988; Ollinger et al., 2002), poor soil conditions (Pickett & Cadenasso, 2009; Rahman et al., 2011; Roman & Scatena, 2011), management choices (e.g., road salting, extensive pruning, and removal of hazard trees; Roman & Scatena, 2011), the amplified impacts of heat waves (Li & Bou-Zeid, 2013; Teskey et al., 2014), abundance of invasive species (Ives et al., 2016; Kühn et al., 2004), and unique wildlife pressures (i.e., deer herbivory; Bressette & Beck, 2013). Soil respiration rates can also be reduced due to high levels of impervious surfaces in urban centers resulting in less soil area being connected to the atmosphere (Decina et al., 2016) and due to the removal of carbon substrates (i.e., leaf litter; Templer et al., 2015).

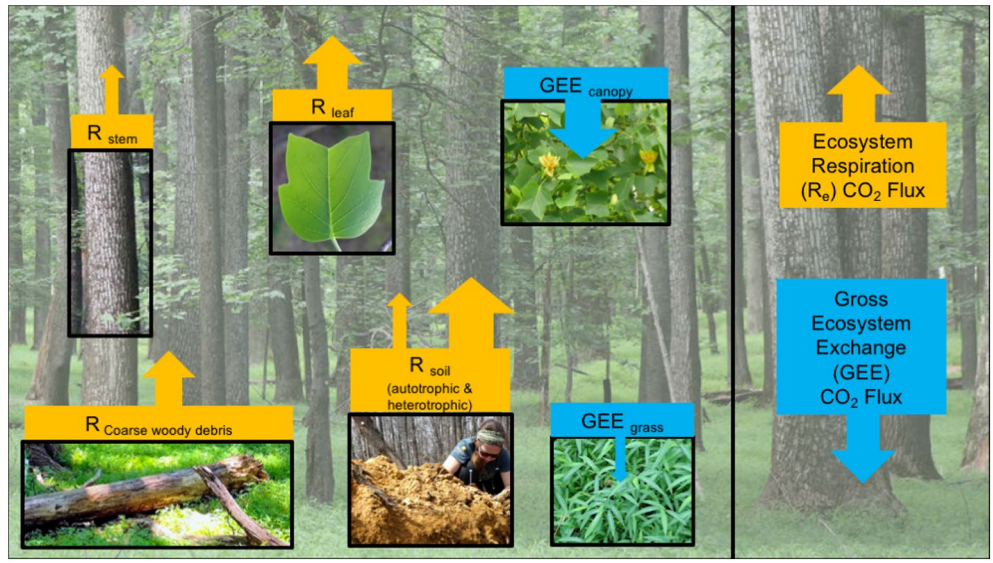

Figure 1. Image of forest field site illustrating the dominance by large Tulip trees (*Liriodendron tulipifera*) and blanket of invasive Japanese stilt-grass (*Microstegium vimineum*) on the forest floor. Boxes represent major ecosystem respiration fluxes (in yellow) and gross ecosystem exchange (GEE) (in blue) quantified in the carbon inventory at forest site. The width of arrows indicate relative size of each flux to total R_e or GEE, respectively.

The key determinant of biogenic CO_2 fluxes among and within urban areas is variation in vegetation type, canopy extent, and management practices. Urban greenspaces are inherently heterogenous with different vegetation types (e.g., trees vs. grasses) receiving different degrees of management (e.g., irrigation, pruning/mowing, mulching, fertilizer), and existing across a spectrum of urban intensities (e.g., street trees in the urban core vs. residential forest patches or city parks) that collectively impact the magnitude of CO_2 flux dynamics. An understanding of how these different greenspaces cycle C is important to obtaining temporally and spatially robust CO_2 flux estimates needed to guide and test policy decisions (Hutyra et al., 2014).

The current generation of ecosystem and climate models used by the scientific community to estimate biogenic CO_2 fluxes were not developed, parameterized, or validated to effectively capture urban areas. Several process-based models developed and parameterized for natural ecosystems have been applied to urban areas, however, they often lack high temporal frequency (e.g., hourly flux estimates), require complex parameter specification, and incur significant computational effort (Churkina, 2008). The models currently under development have varying process-based and management details relevant to urban areas, including those operating at the individual tree scale such as i-Tree (formerly referred to as UFORE; Nowak, 2020), remote-sensing driven models like Urban-VPRM (Urban Vegetation Photosynthesis Respiration Model; Hardiman et al., 2017), and first order models such as ICLEI—Land Emissions And Removals Navigator tool (https://icleiusa.org/learn/). Some flux studies have related seasonal patterns to land cover variability (e.g., urban vegetation) only in broad, qualitative terms or to spatially limited areas (i.e., immediately surrounding a flux tower), which limits city-scale understanding of the urban C cycle (Bergeron & Strachan, 2011; Crawford et al., 2011; Helfter et al., 2011; Järvi et al., 2012; Kordowski & Kuttler, 2010). At the global scale, Churkina (2016) estimated C fluxes of urban areas based on calculating uptake and respiration rates for vegetation and other contributors of the urban C cycle by multiplying the urban extent with the fraction of greenspace in urban areas globally and the gross CO_2 uptake rates of urban vegetation, but assuming uptake rates of a temperate humid forest (Luyssaert et al., 2007). Similarly, most existing ecosystem C exchange models have been developed and parameterized for grassland, agricultural, and forest ecosystems and then modified for application to urban systems assuming urban vegetation responses to environmental conditions in a similar manner as vegetation in rural settings. This assumption has proven incorrect on many occasions (Hardiman et al., 2017; Hutyra et al., 2014; Kaye et al., 2005; Smith, Dearborn, & Hutyra, 2019).

Light-use efficiency models based on remotely sensed data, such as the Vegetation Photosynthesis and Respiration Model (VPRM; Mahadevan et al., 2008), show promise in providing accurate estimates of biogenic CO_2 fluxes at high temporal and spatial resolution, while remaining computationally tractable. It is important to note,

however, that light-use efficiency models are not mechanistic in nature and cannot provide insights into drivers of C storage dynamics but rather help to quantify C flux dynamics. The VPRM was modified by Hardiman et al. (2017) to include factors unique to urban C cycling, in particular the fraction of impervious surface area (ISA) and impacts of urban heat island on air temperatures. The VPRM generates estimates of GEE based on light-use efficiency and ecosystem respiration based on phenology and air temperature (or soil temperature in some cases; Luus & Lin, 2015) using a combination of remote sensing products, such as the enhanced vegetation index (EVI) or normalized difference vegetation index (NDVI) and meteorological data on temperatures and photosynthetically active radiation (PAR). The spatial resolution of the model is based on the remote sensing data products with 500 m Moderate Resolution Imaging Spectroradiometer (MODIS) being more commonly used (Hardiman et al., 2017). However, 30 m Landsat data or 10 m Sentinel-2 data could also be used and in doing so generate spatial estimates of biogenic CO_2 fluxes that better capture the heterogenous growing conditions of urban greenspaces. The VPRM has been parameterized for a range of forest types, agricultural, and grassland ecosystems and has been extended to deciduous forests (Hardiman et al., 2017; Mahadevan et al., 2008), agricultural-urban systems (Lauvaux et al., 2020), arid systems (Park et al., 2018), urban mediterranean systems (Parazoo et al., 2021), and recently run across continental scales for eastern United States and Canada (Gourdji et al., 2021). In all cases the model requires only four parameters per vegetation type, compared to, for example, the 56+ parameters required by the processed based SiB4 land model (Haynes et al., 2019). Furthermore, VPRM has been found to outperform these other process-based models (e.g., SiB4 and CASA) in explaining CO_2 variability (Gourdji et al., 2021). Validation efforts of the VPRM have focused on areas with eddy covariance towers and, to our knowledge, has not been critically evaluated in an urban landscape using field based inventories of biogenic CO_2 fluxes.

Here, we present both field observations and modeled estimates of biogenic CO_2 fluxes in a fragmented urban temperate forest and unmanaged grassland to understand the influence of urbanization on C dynamics. In the case of the forest site, we offer an evaluation of the Urban-VPRM in this context. Specifically, we test the following hypotheses at the FOREST (Forested Optical Reference for the Evaluation of Sensor Technology) site on the National Institute of Standards and Technology (NIST) urban campus in Gaithersburg, Maryland. First, we hypothesize that the novel conditions created by urbanization will result in urban vegetation acting as a net sink for atmospheric CO_2 with notable temporal variability in C storage and CO_2 flux dynamics. We test this hypothesis with a field-base CO_2 inventory in study plots established at the FOREST site and adjacent unmanaged grassland. Second, we hypothesize that the VPRM will closely approximate GEE and R_e dynamics observed in the CO_2 FOREST inventory. We will test this hypothesis by running the Urban-VPRM for the same forest patch area in which our field-based inventory plots are located, identifying key areas in need of model development. Third, we hypothesize that CO_2 flux dynamics will vary seasonally between the forest patch and unmanaged grassland. We will test this hypothesis by examining the temporal dynamics in CO_2 fluxes generated by the Urban-VPRM for the areas overlapping the FOREST patch and adjacent unmanaged grassland. Lastly, we will examine how net biogenic CO_2 fluxes influence temporal and spatial patterns in net flux dynamics (biogenic + FF) by expanding the spatial scope of our study to a 6 km^2 area around the FOREST site. Broadly we predict the region will be a net source of CO_2 driven by FF emissions, however, by examining the fine spatial and temporal scale of flux dynamics, we expect to identify when and where urban vegetation strongly impacts net CO_2 flux dynamics in the study region.

2. Materials and Methods

2.1. Overview

Our study examines the structure and function of urban forest patch and unmanaged grassland as it pertains to CO_2 fluxes and aboveground C storage using biometric measurements. Our field site is located at the NIST urban campus in Gaithersburg, Maryland (Figure 2) in the FOREST plot (Figure 2a) and adjacent unmanaged grassland. We present for the FOREST and grassland study plots annual estimates of C dynamics (Table 1). In the case of the FOREST plot where we had a higher frequency of measurements, we present hourly estimates of all major CO_2 fluxes and compare them to modeled estimates of biogenic CO_2 fluxes using the Urban-VPRM model. We compare hourly estimates from the Urban-VPRM for the FOREST and grassland study areas to examine differences in CO_2 fluxes among these different land use types. To explore the temporal and spatial significance of biogenic CO_2 fluxes relative to anthropogenic FF emissions of CO_2 we expanded the scale of the Urban-VPRM analysis

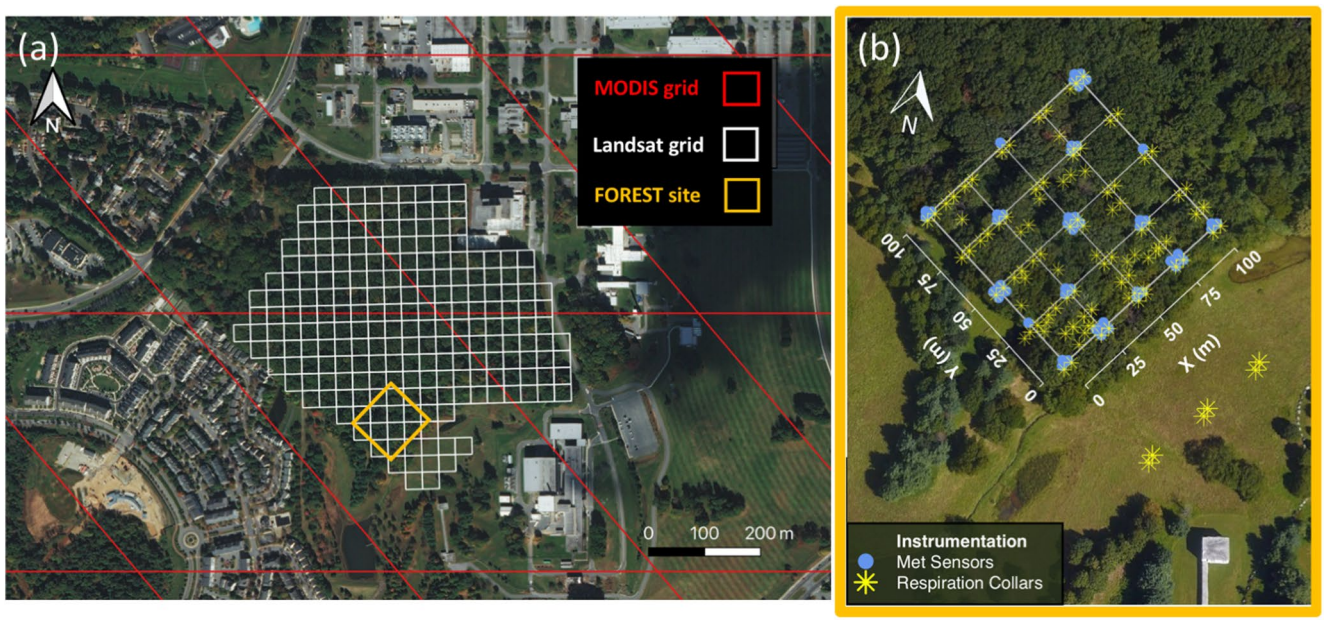

Figure 2. Panel (a) shows an aerial image illustrating the spatial extent of analysis. The Landsat grids (shown in white) correspond to those used when comparing Vegetation Photosynthesis and Respiration Model (VPRM) estimates to field inventory estimates of CO_2 fluxes. An example of 500 m Moderate Resolution Imaging Spectroradiometer grids (shown in red) are shown to illustrate how the 30 m run of the VPRM compares to traditional scale at which the model is run (Mahadevan et al., 2008). The Forested Optical Reference for the Evaluation of Sensor Technology (FOREST) site is shown in yellow. Panel (b) shows a zoomed in map of the 1 ha FOREST site and location of grassland study plots. The location of study instrumentation for meteorological observations are shown in blue and soil respiration measurements are shown in yellow.

to a 6 km^2 area around the FOREST site to examine the combined effect of biogenic and FF sources of CO_2 on net flux dynamics. In all cases, we ran a modified version of the Urban-VPRM to estimate biogenic CO_2 fluxes at 30 m resolution. While the original formulation of the VPRM was run at 500 m (Mahadevan et al., 2008), the

Table 1
Biogenic Carbon Dioxide Flux Estimates Computed Using the Field-Based Inventory and the Urban-VPRM Model for the Forest and Grassland Site for Both an Annual Time Period and the Summer Months of June, July, and August (JJA)

Site	Forest				Grassland	
Time period	Annual		JJA			
Estimate	Inventory	VPRM	Inventory	VPRM	Inventory	VPRM
Ecosystem respiration						
Coarse woody debris	1.40 ± 0.28	–	0.60 ± 0.07	–	–	–
Heterotrophic soil	3.62 ± 1.1	–	1.57 ± 0.28	–	–	–
Total heterotrophic	5.02 ± 1.2	–	2.17 ± 0.29	–	–	–
Autotrophic soil	0.904 ± 0.28	–	0.39 ± 0.07	–	–	–
Autotrophic stem	0.890 ± 1.0	–	0.37 ± 0.25	–	–	–
Autotrophic leaf	2.77 ± 0.80	–	1.35 ± 0.19	–	–	–
Total autotrophic	4.56 ± 1.4	–	2.11 ± 0.32	–	–	–
Total	9.58 ± 1.8	11.70	4.28 ± 0.43	4.17	2.08 ± 0.59	1.32
Gross ecosystem exchange						
Canopy	−12.2 ± 0.63	−12.6	−7.95 ± 0.16	−9.13	−6.94 ± 0.57	−5.23
Net ecosystem exchange	−2.62 ± 1.9	−0.91	−3.67 ± 0.46	−4.97	−4.86 ± 0.82	−3.91

Note. Fluxes are reported in units of Mg C ha^{-1} yr^{-1} ±error. Error is shown as the root mean square error. Total uncertainty in net ecosystem exchange estimates is computed as the root mean square of component errors.

30 m resolution better captured fine-scale spatial heterogeneity prevalent in urban systems. This allowed for distinction between fluxes across patches of unmanaged grasslands and forested areas. In the case of the FOREST site, this allowed for a direct comparison to hourly field inventory estimates of biogenic fluxes thereby providing critical evaluation of the Urban-VPRM in this ecosystem.

Figure 1 summarizes the major CO_2 fluxes empirically quantified to compute the GEE and R_e estimates. Negative fluxes represent gross carbon uptake or GEE while positive fluxes represent releases of carbon to the atmosphere or R_e. NEE is the difference between GEE and R_e. Fluxes are reported as μmols CO_2 m^{-2} s^{-1} when presenting daily or hourly estimates and are reported as Mg C ha^{-1} when presenting seasonal or annual estimates. We report CO_2 fluxes at the grassland site for the summer months of June through August when measurements were actively being made and present those as a cumulative flux (Mg C ha^{-1}; Table 1). We do not present hourly estimates in the grassland plots due to the lack of temporally resolved estimates of grassland leaf area. Conversely, in the FOREST site we report daily mean fluxes (μmols CO_2 m^{-2} s^{-1}), in addition to cumulative flux estimates for the summer months of June through August (Mg C ha^{-1}) and for the entire year (Table 1).

2.2. Biometric Measurements

2.2.1. Site Description and Meteorological Variables

In May 2017, a 100 m by 100 m plot was established along the edge of the 26 ha forest fragment at the FOREST site. In May 2018, three 1 m by 1 m plots were established in the adjacent unmanaged grassland (Figure 2b). The FOREST plot is a *Liriodendron tulipifera/Quercus* sp. dominated stand with a 3 m wide stream flowing through the plot approximately 25 m from the forest edge. The forest edge of the plot has a southeastern aspect with a west facing "soft" edge with low stem density (Figure 2b). The forest understory is dominated by Japanese stiltgrass (*Microstegium vimineum*), a highly productive invasive annual grass common in many urban forests of the eastern United States (Averill et al., 2017). The site has a high density of deer with an estimated 85 individuals km^{-2} in 2017 (Rutberg & Naugle, 2008). Soils are classified as Glenelg series silt loam with a high clay content and low levels of soil organic matter (Natural Resources Conservation Service, 2018). Mean summer (June through August) air temperatures are 23.5°C and mean winter (December to February) air temperatures are 1°C. Mean annual precipitation are 1,093 mm and evenly distributed throughout the year (National Climatic Data Center, 2018).

The FOREST and grassland plots were instrumented with sensors measuring relative humidity, air and soil temperature, and soil moisture (Figure 2b). Soil temperature and moisture were logged hourly at a depth of 10 cm. Soil temperatures were measured with Onset HOBO Pendant Dataloggers at 11 locations ($n = 22$) across the FOREST plot and one location in the grassland plots. Soil moisture was measured with Onset HOBO Soil Moisture Smart Sensors at five locations across the FOREST plot and one location in the grassland study area. Air temperature and relative humidity were measured hourly with HOBO Data Loggers at 14 locations in the FOREST plot and at one location in the grassland study area. PAR data was derived from the Geostationary Operational Environmental Satellite-16 (GOES-16) level 1b radiances for 2018 at a spatial resolution of 0.05° by 0.05° and hourly temporal resolution (EUMETSAT OSI SAF, 2021, 2018). We found that the GOES-16 PAR data closely approximated available site-level PAR conditions measured for part of the summer using Onset HOBO PAR Smart Sensor (Figure S1 in Supporting Information S1).

2.2.2. Carbon in Standing Biomass

Aboveground biomass (AGB) in vegetation was quantified using allometric equations based on tree diameters at 1.37 m height (i.e., diameter at breast height or DBH). In May 2017, all trees in the plot with stems >5 cm DBH were tagged and DBH was recorded, including standing snags. In November 2019, a re-survey of tree DBH was conducted to estimate tree mortality, recruitment of new stems with DBH >5 cm, and contributions to the CWD pool. To minimize remeasurement error between years in DBH estimates, the height of DBH measurement of each tree was marked with the nail of each tree tag and all trees in the plot were remeasured. During the re-survey, on a subset (approximately 10% of trees) two researchers measured DBH to reduce measurement error. Aboveground forest carbon stocks were estimated using DBH-based allometric equations on an inventory of all tree stems greater than 5 cm. The allometric equations by Chojnacky et al. (2014) were used in all cases except for the tree species *L. tulipifera*. The site included 21 very large *L. tulipifera* trees which exceeded the range of tree sizes (up to 65 cm) from the Chojnacky et al. (2014) allometric equations, potentially causing an over-estimate of standing biomass. To account for this, we used allometric equations from Stoval et al. (2018) for the *L. tulipifera*

trees which were derived using LiDAR for a mature *L. tulipifera* dominated forest stand nearby the FOREST site (145 km west). This approach reduced the C in AGB estimate by 3.31 Mg C ha^{-1} yr^{-1} or a 1.1% difference in AGB estimates.

The AGB in the unmanaged grassland were quantified through destructive harvest in September 2018. We harvested all AGB from two, 25 cm by 25 cm subplots adjacent to each of the three grassland plots described above. The biomass was separated into four categories: litter, green leaves, green stems, and brown leaves/stems, which reflects current year necromass associated with mid-growing season senescence common in temperate mesic grasslands (e.g., Hutchison & Henry, 2010). Samples were dried at 60°C to a constant weight to quantify dry biomass.

At the end of the 2019 summer, a survey was conducted to estimate the AGB of *M. vimineum* and its contribution to total forest net primary productivity. To calculate AGB, plant material was harvested from 25, 0.5 m by 0.5 m plots located on a 25 m by 25 m grid across the FOREST site. The samples were oven-dried at 60°C and weighed (±0.0005 g). *M. vimineum* density distribution was assessed on the day of harvest using a quadrat frame approach. Briefly, using this method 0.5 m by 0.5 m density sampling plots were laid out on a 6.25 m by 6.25 m grid across the FOREST site ($n = 289$; Figure S2 in Supporting Information S1). Density was assigned into one of the following categories, based on the area covered by *M. vimineum* inside the quadrant frame, 0%, 1%–25%, 26%–50%, 51%–75%, and 76%–100%.

In all cases, carbon stocks were estimated assuming the dry AGB biomass was 50% carbon (Fahey et al., 2005).

2.2.3. Gross Ecosystem Exchange

GEE, or the total uptake of CO_2 from the atmosphere to the ecosystem, was computed in the FOREST and grassland site by using a big-leaf modeling approach (Sprintsin et al., 2012).

As an methodological overview, leaf-level estimates of gross photosynthesis are estimated from a model that uses the relationship between direct measurements of net photosynthesis across a range of PAR conditions (i.e., light response curves or LRC). Gross photosynthesis is the product of net photosynthesis plus leaf respiration. The hourly estimates of leaf-level gross photosynthesis (μmol CO_2 m^{-2} leaf area s^{-1}) use hourly PAR data derived from GOES-16 (EUMETSAT OSI SAF, 2021). PAR data from GOES could result in an underestimate of gross photosynthesis due to inaccuracies associated with cloud conditions, however cloud conditions are accounted for in the algorithm used to compute solar surface irradiance and estimates are validated with *in-situ* instrumentation with good agreement ($R^2 = 0.95$; EUMETSAT OSI SAF, 2018). Indeed, the GOES-16 derived PAR closely approximates available site-level PAR conditions during the summer months on both sunny and cloudy days (Figure S1b in Supporting Information S1). Estimates of gross photosynthesis are then scaled to the entire canopy (μmol m^{-2} ground area s^{-1}) using the leaf area index (LAI) of the ecosystem. These estimates are adjusted using Beer's law to account for light decay through the canopy (or the difference in top of canopy versus leaf-level PAR conditions), and changes in light use efficiency of the leaves. Estimates were scaled across the entire growing season by accounting for seasonal changes in LAI and LUE. We assume there are no seasonal changes in the light decay through the canopy.

Gross leaf-level photosynthesis were estimated from light-response kinetics where net photosynthesis is directly measured over a range of PAR conditions. Photosynthetic LRC were fitted to a non-rectangular hyperbola model using non-linear least square techniques as described in Lambers et al., 2008 (Figure S3 in Supporting Information S1) and this model was used to generate estimates of gross photosynthesis. LRC were measured on the five most dominant tree canopy species including *Acer rubrum*, *Quercus alba*, *Carya tomentosa*, *Fraxinus americana*, and *L. tulipifera* (Figure S3 in Supporting Information S1). These species collectively account for 93% of the AGB in the study plot (Figure S4a in Supporting Information S1). Due to canopy access constraints, LRC were conducted on forest edge trees. The weighted mean of the LRC kinetics for the five species was computed based on the relative contribution to the total AGB in the FOREST plot (Figure S4a in Supporting Information S1) and assumed to be homogenous throughout the canopy.

In the FOREST and grassland, LRC of photosynthetic CO_2 assimilation across a range of PAR conditions were measured using a LI-COR 6800 photosynthesis analyzer with the 6800-01A fluorometer head (LI-COR Bio-Sciences, Lincoln, NE, USA). All leaves were full-sun acclimated and measured at a reference CO_2 concentration of 400 μL L^{-1}, a chamber air temperature of 30°C, and a vapor pressure deficit of 2. Conditions were intended

to simulate ambient conditions for parameters other than temperature, which was set slightly above ambient to reduce the risk of condensation within the instrument. Leaves were permitted to equilibrate for 2–5 min to a given light intensity before measurements were recorded. In the forest, these LRC were measured between 31 July and 3 August 2017 (i.e., peak growing season) while in the grassland they were conducted on 12 June, 6 August, and 22 August 2018. In the grassland sites LRC were conducted on two grass blades per study plot for a total of 18 leaf samples for the summer of 2018. June sampling was used to represent all days in the months of June and July while the August sampling was used for all days in the month of August.

Hourly estimates of gross photosynthesis (A_{leaf}) were scaled to the entire forest area (A_{canopy}) using Beer's Law (light decay through the canopy) and daily changes in LAI (Equation 1). The canopy PAR extinction coefficient (k) was derived from the meta-analysis by L. Zhang et al. (2014) using the average deciduous forests value of 0.59 and average grassland value of 0.50.

$$A_{canopy} = A_{leaf} * (1 - \exp(-k * LAI)) \quad (1)$$

In the grassland, LAI was assumed to be 2.0 throughout the growing season (Asner et al., 2003). Due to the lack of a temporally resolved estimate of LAI or LUE in the grassland, we do not present hourly estimates of grassland CO_2 fluxes but rather only present cumulative estimates for the peak part of the growing season (July through August). Conversely, seasonal changes in LAI in the FOREST was computed using multiple approaches to develop the best approximation for our field site (Figure S5a in Supporting Information S1). First, the PhenoCam measurements at the NIST site were used to determine start and end dates for the growing season (Richardson et al., 2018; Figure S5b in Supporting Information S1). Second, NDVI was retrieved at the NIST site for 139 days during 2018 using the Harmonized Landsat and Sentinel-2 surface reflectance data set (HLS; Claverie et al., 2018) V1.4. HLS data was cloud-filtered and interpolated between collection dates using a spline function. Third, data was extracted on key land surface phenology thresholds for the NIST site from the Multi-Sensor Land Surface Phenology product to estimate the length of the growing season (Bolton et al., 2020; Figure S5a in Supporting Information S1). Finally, we developed a seasonal LAI scalar using LAI observations from a nearby (~84 km east) *L. tulipifera* dominated forest stand at SERC (Smithsonian Environmental Research Center) in Anne Arundel County, Maryland (National Ecological Observatory Network [NEON], 2020). Briefly, LAI estimates from SERC were obtained by processing raw digital hemispherical photos from 13 time points from April through October (twice per month) and were processed using the Gap Light Analyzer software version 2.0 (Frazer et al., 1999). In the main text, estimates using the SERC LAI scalar are presented, however, in the results we discuss how the scalars compared.

The SERC- and NDVI- derived scalars were normalized to our only field estimate of LAI (value of 3.84) at the FOREST site, taken on 2 August 2018 (Figure S5a in Supporting Information S1). This approach assumed our August sampling was representative of spatial variability throughout the growing season. Our August estimate of LAI was taken using hemispherical photos collected at a height of one meter above the forest floor using a full-frame DSLR camera equipped with a fisheye lens. Photos were processed using the Gap Light Analyzer software version 2.0 (Frazer et al., 1999) where analysis was restricted to a 53° zenith angle toward the forest interior to minimize the influence of lateral light penetration in photos collected near the forest edge. LAI measurements were collected on a 12.5 m grid across the entire FOREST site ($n = 81$ measurements) and the mean value was 3.84 ± 0.08 SE.

The LUE scalar used in the big-leaf modeling approach for the FOREST study plot (Figure S6 in Supporting Information S1) was estimated from the Duke Forest hardwood eddy covariance flux tower located in Durham, North Carolina (described in Section 2.3) by examining GEE estimates during the growing season at controlled PAR levels. LUE was approximated by computing biweekly average GEE under conditions where PAR was between 1,000 and 1,600 μmol m^{-2} s^{-1}. Scalars were then determined across the growing season by dividing the biweekly average LUE under controlled PAR conditions by the maximum observed biweekly LUE. To account for differences in latitude, the data was offset by 10 days to constrain the scalar to the shorter growing season observed in Gaithersburg, Maryland compared to Durham, North Carolina.

2.2.4. Ecosystem Respiration

Ecosystem respiration (R_e), or the release of CO_2 from the ecosystem to the atmosphere, was computed in the FOREST plot as the sum of autotrophic and heterotrophic sources of CO_2 fluxes. Empirically derived fluxes of

autotrophic respiration included estimates of respiration by tree leaves, tree stems, and the fraction of soil respiration that is from roots/symbionts. Heterotrophic respiration in the forest was the sum of CO_2 flux from CWD and the heterotrophic portion of soil respiration. In the grassland plots, R_e was the sum of soil and leaf respiration.

Leaf or canopy respiration in the FOREST and grassland plots were estimated using the dark respiration estimates from the *y*-intercept in the LRC (as described in Section 2.2.3; Figure S3 in Supporting Information S1; Lambers et al., 2008). The Kok effect on daytime leaf respiration was accounted for by assuming daytime leaf respiration was 40% of dark respiration (Wehr et al., 2014). Leaf respiration estimates were scaled from the leaf-level (what is estimated from the LRC) to the entire canopy using Equation 1, except A_{leaf} is replaced with leaf-level estimates of respiration from the LRC.

Stem respiration was quantified in the FOREST, but not the grassland site where it was assumed to be negligible. In the FOREST, stem respiration was measured on 22 tree stems that are distributed across the 1 ha plot among the dominant tree species and capturing range of tree sizes. On each stem a 15.5 cm diameter by 7 cm tall respiration collar was affixed at approximately 1.3 m above the ground with non-greenhouse gas emitting silicone sealant. Fluxes were quantified with LI-COR LI-840A CO2 gas analyzer following the vented design described by Savage and Davidson (2001) roughly every 2 weeks during the growing season. Stem respiration fluxes (units μmols CO_2 m^{-2} stem area s^{-1}) were estimated for each tree stem in the plot >5 cm using a linear regression model with chamber temperature, DBH of the tree in 2019, and distance from forest edge. Stem respiration per tree stem (μmols CO_2 s^{-1}) was computed with estimates of the total stem surface area of each tree in the plot that had a DBH >5 cm using allometric equations in Martin et al. (1998).

In the FOREST plot, soil respiration measurements are described in Smith, Hutyra, et al. (2019). An additional two soil collars were placed in each of the three grassland plots ($n = 6$ collars total). In all cases, soil respiration was measured on 15.5 cm diameter by 7 cm tall respiration collars that were inserted into the ground 2 cm using a LI-COR LI-840A CO_2 gas analyzer following the vented design described by Savage and Davidson (2001). Measurements in both the FOREST and grassland plots were made between May and October roughly every 2 weeks in 2018 and 2019. For the FOREST plot, soil respiration measurements were scaled to the entire year using a linear regression model with soil temperature, soil moisture, and distance from forest edge. For the grassland, soil respiration values were scaled June through August using a linear regression model with relationship of empirical estimates of soil respiration measured in both 2018 and 2019 with soil temperature. Prior studies have shown that annual soil respiration fluxes can be estimated from year-round measurements of soil moisture and temperature (Davidson et al., 1998; Giasson et al., 2013; Rey et al., 2002). Smith, Hutyra, et al. (2019) demonstrated a strong edge effect on soil respiration rates at our field site that was accounted for by more intensive sampling near forest edges (Figure 2b). In the FOREST, we assumed 20% of the soil respiration flux is autotrophic (Hanson et al., 2000).

The CO_2 flux from CWD was estimated using an air temperature-driven respiration model across decay classes presented in Liu et al. (2006). Coarse wood debris pools were quantified in the summer of 2017 using the line-intercept method (Van Wagner, 1968). Additional contributions to the standing or fallen CWD pool between 2017 and 2019 were quantified with DBH resurvey by identifying trees that had fallen since 2017 or became snags. Error on the CWD pool was estimated as standard deviation among 46, 10 m transects used in the line-intercept method. Transects were distributed throughout the 1 ha plot along the south facing edge including 10 transects along the southern facing edge (shown in Figure 2b), seven transects at 25 m in from the southern edge, nine transects at 50 m from the southern edge, and 10 transects at 75 and 100 m from the southern forest edge. Note, our estimates of CWD flux do not account for potential edge effects on decomposition which has been reported to reduce rates of decomposition because of drier conditions (Crockatt & Bebber, 2015).

2.3. Urban-VPRM Model

The VPRM is a spatially explicit, data driven model that produces hourly estimates of ecosystem exchange of CO_2 using remote sensing and climate analysis data products (Mahadevan et al., 2008). We ran a modified version of the Urban-VPRM (Hardiman et al., 2017) that included the suppression of respiration rates by presence of ISA in urban areas. Additionally, we modified the T_{scale} to provide a range of temperatures (20°C–30°C) that are optimal for photosynthesis rather than a fixed value as is the case in original version of Urban-VPRM. This was

done to capture the higher and greater range of temperatures at which photosynthesis remains to be optimized (Figure S7b in Supporting Information S1).

Below we present the necessary model equations and data specifications to apply the modified version of the Urban-VPRM (summarized in Table S1 in Supporting Information S1). Model equations were executed in R version 3.6 (R Core Team, 2020). Model code with example driver datasets is archived at http://doi.org/10.7910/DVN/UNF7EB.

In the Urban-VPRM, GEE is estimated using the following equation:

$$\mathrm{GEE} = -1 \times \lambda \times T_{\mathrm{scale}} \times P_{\mathrm{scale}} \times W_{\mathrm{scale}} \times \mathrm{EVI} \times \frac{1}{1 + \frac{\mathrm{PAR}}{\mathrm{PAR}_0}} \times \mathrm{PAR} \tag{2}$$

where T_{scale}, P_{scale}, and W_{scale} are dimensionless scaling terms ranging from zero to one describing the influence of air temperature, phenology, and moisture on photosynthesis. PAR is photosynthetically active radiation (μmol m^2 s^{-1}). λ and PAR_0 are plant functional type-specific parameters describing the maximum quantum yield (μmol CO_2 μmol PAR^{-1}) and half-saturation value (μmol m^2 s^{-1}) of the light-use efficiency curve. EVI is the Enhanced Vegetation Index.

The modified T_{scale} is computed as:

$$\begin{cases} \text{if } T < 20;\ T_{\mathrm{scale}} = \dfrac{(T - T_{\min})(T - T_{\max})}{(T - T_{\min})(T - T_{\max}) - (T - 20)^2} \\ \text{if } 20 \le T \le 30;\ T_{\mathrm{scale}} = 1 \\ \text{if } T > 30;\ T_{\mathrm{scale}} = \dfrac{(T - T_{\min})(T - T_{\max})}{(T - T_{\min})(T - T_{\max}) - (T - 30)^2} \end{cases} \tag{3}$$

where T is the air temperature, T_{min} is the minimum temperature for photosynthesis (0°C), and T_{max} is the maximum temperature for photosynthesis (40°C).

P_{scale} captured the impact of leaf age on vegetation activity and were calculated as:

$$P_{\mathrm{scale}} = \frac{\mathrm{EVI} - \mathrm{EVI}_{\min}}{\mathrm{EVI}_{\max} - \mathrm{EVI}_{\min}} \tag{4}$$

where $\mathrm{EVI}_{\min}$ and $\mathrm{EVI}_{\max}$ are the minimum and maximum observed EVI for each pixel during the growing season.

W_{scale} is a function of the Land Surface Water Index (LSWI) which has been shown to be effective in monitoring vegetation water content (Gu et al., 2008; Maki et al., 2004) and is calculated as:

$$W_{\mathrm{scale}} = \frac{1 + \mathrm{LSWI}}{1 + \mathrm{LSWI}_{\max}} \tag{5}$$

where $\mathrm{LSWI}_{\max}$ is the maximum LSWI observed for a given pixel during the growing season.

R_e was computed using equations presented in Hardiman et al., 2017 that are reproduced below. First, R_e is calculated as a linear function of temperature:

$$R_{e,\mathrm{init}} = T \cdot \alpha + \beta \tag{6}$$

where T is the air temperature (°C), α is the sensitivity of R_e to T, and β is the minimum value that $R_{\mathrm{eco,\ init}}$ can take on (μmol CO_2 m^{-2} s^{-1}). The heterotrophic respiration component flux is then adjusted to account for restricted diffusion of CO_2 due to the sub-pixel proportion of ISA as:

$$R_H = (1 - \mathrm{ISA}) \times \frac{R_{e,\mathrm{init}}}{2} \tag{7}$$

EVI is used as a proxy for the amount of living biomass and the associated autotrophic respiration within a pixel. Therefore, the autotrophic respiration component flux was scaled by pixel greenness as:

$$R_A = \left(\frac{\mathrm{EVI} + \mathrm{EVI}_{\mathrm{ref,min}} \times \mathrm{ISA}}{\mathrm{EVI}_{\mathrm{ref}}}\right) \times \frac{R_{e,\mathrm{init}}}{2} \quad (8)$$

where $\mathrm{EVI}_{\mathrm{ref}}$ is the EVI at a non-urban reference site. $\mathrm{EVI}_{\mathrm{ref,min}}$ are the minimum observed EVI at the reference site, representing a baseline leaf-off, woody biomass respiration. The final value of R_e was then calculated as the sum of the two component fluxes R_H and R_A.

VPRM driver data come from publicly available remote sensing and modeling products. A summary of model parameters and their data sources and estimated values can be found in Table S1 in Supporting Information S1. We used the AmeriFlux Duke Forest hardwood and open field towers (Oishi et al., 2018; AmeriFlux IDs: US-Dk1 & US-Dk2) to estimate VPRM coefficients for forests and grasslands due to similarities with the FOREST site in species composition, stand age, and climate (Stoy et al., 2005). In the GEE equation, λ and PAR_0 are optimized via nonlinear least squares regression using eddy covariance flux tower measurements of CO_2 flux and PAR between 2001 and 2008 from US-Dk AmeriFlux sites. T_{scale} is derived from observations of growing season photosynthesis and temperature at US-Dk2 (Figure S7a in Supporting Information S1). In the R_e equation, β was set to the minimum observed R_e at the FOREST site and α was determined using linear regression and observations from the US-Dk AmeriFlux sites. PAR data came from the GOES-16 (EUMETSAT OSI SAF, 2021) which provided high spatial (0.05° by 0.05°) and temporal (hourly) resolution of incoming shortwave radiation (Watts m^{-2}). PAR was approximated to be shortwave radiation divided by 0.505 (Mahadevan et al., 2008). EVI and LSWI are calculated from the Landsat 7 and Landsat 8 Tier 1 Surface Reflectance Products (Masek et al., 2006; Vermote et al., 2016). Using data from two Landsat sensors allows for EVI to be obtained every eight days. Daily EVI and LSWI values are interpolated between collection dates using a spline function. Green-up and dormancy dates where acquired from Multi-Source Land Imaging Land Surface Phenology (MSLSP30NA) product for North America derived from HLS data at a 30 m resolution (Bolton et al., 2020). ISA data came from the National Land Cover Database imperviousness product (Homer et al., 2015) at a 30 m resolution. Air temperature data came from the Rapid Refresh analysis product (Benjamin et al., 2016) at a spatial resolution of 13 km by 13 km and temporal resolution of 1 hr.

2.4. ACES Data

We compared the spatial and seasonal mean diurnal trends in the biogenic CO_2 estimates from the VPRM to CO_2 emissions from FF combustion for the same geographic area of 6 km^2. We derived estimates of FF-CO_2 from the Anthropogenic Carbon Emissions System (ACES) for the Northeastern USA (Gately & Hutyra, 2018). ACES reports emissions from 10 different source sectors at a 1 km gridded resolution and hourly time-step for 2014. ACES emissions from residential, commercial, industrial, railroad, marine vessel, non-road vehicle, airport taxiing, takeoff and landing operations, and electric power generation sources are derived from the United States Environmental Protection Agency National Emissions Inventory (EPA; United States Environmental Protection Agency, 2014a) and the EPA Greenhouse Gas Reporting Program (United States Environmental Protection Agency, 2014b). On-road vehicle emissions were obtained from the Database of Road Transportation Emissions (Gately et al., 2015). Full details of the ACES methodology can be found in Gately and Hutyra (2018). For this study, the 2014 ACES emissions were scaled forward to 2018 accounting for seasonal and daily variations in meteorology, fuel consumption, and traffic patterns across these years. We present spatial trends in the ACES data as mean hourly fluxes for the months of June through August (Figure 7a) and the seasonal trends in diurnal fluxes across the entire spatial domain (Figure 8). We define fall as the months of 1 September to 31 November, Winter as 1 December to 31 March, Spring as 1 April to 31 May, and Summer as 1 June to 31 August.

2.5. Statistical Analyzes

Error was reported as the root mean square error (RMSE) of the empirically derived statistical models used to scale field measurements to area-based estimates (e.g., μmols CO_2 m^{-2} s^{-1} or Mg C ha^{-1} yr^{-1}). In the case of GEE estimates, error was computed as the RMSE of the non-rectangular hyperbola model used to generate net photosynthesis estimates for each LRC. Total uncertainty among LRC (of tree species in FOREST plot, or among grassland plots) was computed by taking the square root of the sum of squared error terms. In the FOREST site error terms were weighted by the relative contribution of each tree species to the total AGB (Figure S4a in Supporting Information S1). Similarly, error for estimates of stem and soil respiration fluxes was computed as the

RMSE of the linear model used to scale these flux measurements to the forest stand. Error on the CWD flux was computed by taking the square root of the sum of squared error terms on error associated with the CWD pool estimate and the error on the decay rate constant in the Liu et al. (2006) respiration model. Lastly, in the FOREST site the error in dark respiration used in the leaf respiration estimate was reported as the standard deviation of the dark respiration measured among the five tree species weighted by the relative contribution of each species to the total AGB (Figure S4a in Supporting Information S1). In the grassland site the error in dark respiration used in the leaf respiration estimate was reported as the standard deviation of the dark respiration measured among the LRC conducted on the three grassland plots. In all cases, total uncertainty in flux estimates was computed as the square root of the sum of squared error terms.

Rigorous analysis of uncertainty and error in the VPRM are summarized elsewhere by Luus and Lin (2015), Lin et al. (2011), and Hilton et al. (2014). In each of these studies error in the VPRM was assessed using measurements of carbon fluxes from eddy covariance flux sites and independent datasets for meteorological driver data. In the case of Luus and Lin (2015) and Lin et al. (2011) this included eddy flux towers in boreal ecosystems. Hilton et al. (2014) assessed VPRM error at the scale of the continental United States using the network of 65 AmeriFlux eddy covariance towers. While some of the AmeriFlux towers are located in urban/suburban areas, eddy covariance approaches are challenging to deploy in urban areas because the heterogenous terrain of urban areas often violates the methodological assumptions of this technique, thereby making it difficult to conduct similar error analysis in urban areas. All statistical analyses and modeling were conducted using R statistical Software 3.6 (R Core Team, 2020).

3. Results

3.1. Biometric Measurements of Carbon Pools and Fluxes

Total AGB carbon pools was estimated as 189.5 and 3.44 ± 0.61 Mg C ha^{-1} in the FOREST and grassland, respectively. The forest floor was covered extensively by Japanese stiltgrass *M. vimineum,* which contributed an additional 0.37 ± 0.07 Mg C ha^{-1} (Figure 3; Figure S2 in Supporting Information S1). AGB in the FOREST is

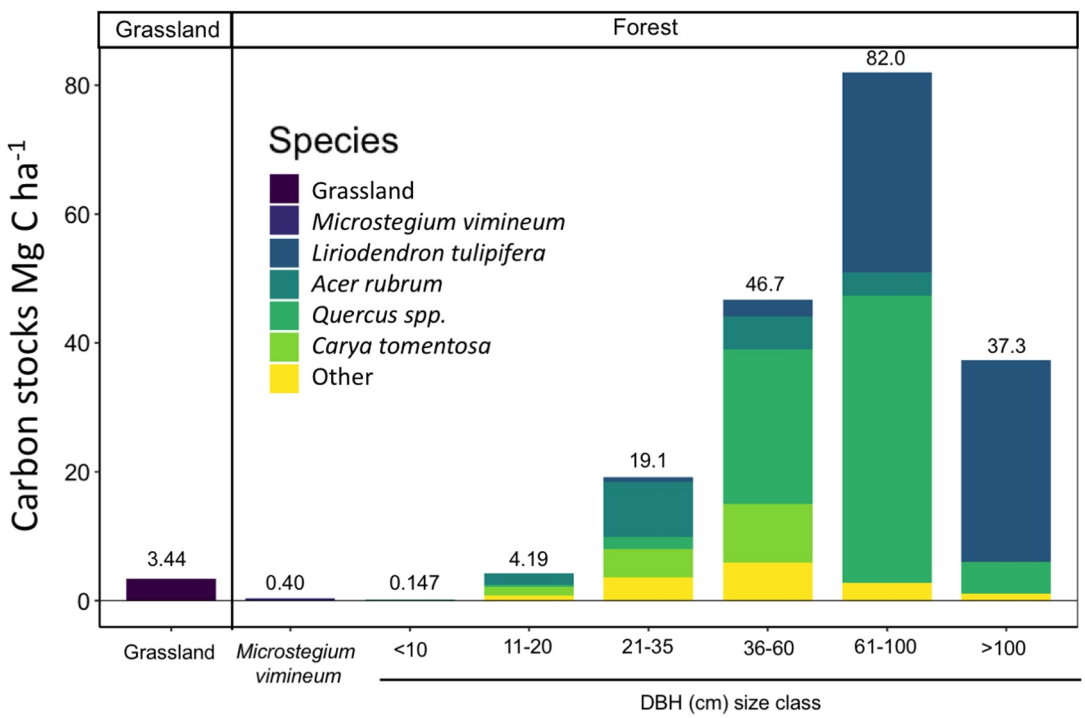

Figure 3. Stacked bar plot showing the aboveground carbon stocks (Mg C ha^{-1}) in the un-managed grassland and Forested Optical Reference for the Evaluation of Sensor Technology (FOREST) site. In the FOREST site, carbon stocks are shown for the dominant tree species by diameter at breast height size class as well as the invasive stiltgrass *Microstegium vimineum* groundcover. The total aboveground carbon stock is shown on the top of each bar.

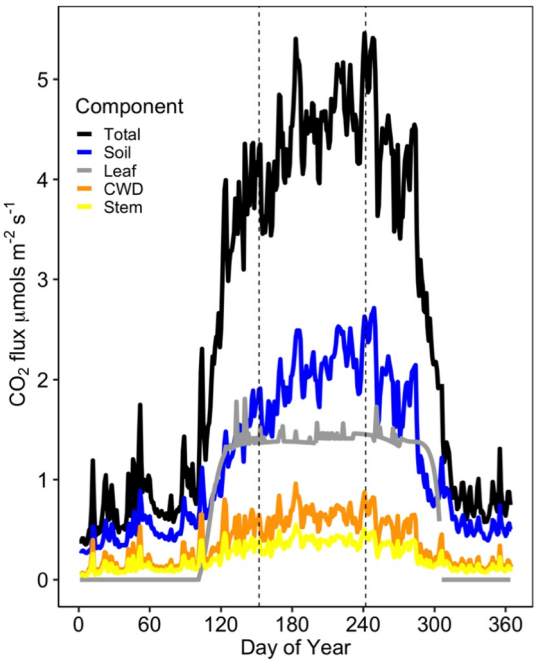

Figure 4. Components of inventory estimate of ecosystem respiration fluxes for the Forested Optical Reference for the Evaluation of Sensor Technology site. The black line represents the total daily mean carbon flux (µmols CO_2 m^{-2} s^{-1}). Colored lines show each contributing component to the total inventory based ecosystem respiration estimate.

dominated by *Quercus* species (40%) followed by *Liriodendron* trees (35%) (Figure 3; Figure S4a in Supporting Information S1). There was no recruitment of stems >5 cm observed between DBH surveys in 2017 and 2019 and low stem density in small DBH size trees suggests a lack of recruitment in the proceeding years as well (Figure S4b in Supporting Information S1). The lack of tree sapling recruitment is despite several canopy gaps having formed from mortality of large trees. An additional 3.4 Mg C ha^{-1} was added to the forest floor CWD pool from tree mortality that occurred between 2017 and 2019. The CWD pool on the forest floor was estimated in 2017 as 7.7 ± 0.3 Mg C ha^{-1}. The total pool of CWD in 2018 was estimated as 11.1 Mg C ha^{-1}.

Using our biometric measurements, we find that the grassland and FOREST site are a net sink for carbon in the summer months of June to August. In the case of the FOREST site, where year-round measurement were made, we find a smaller but sustained annual carbon sink. We present all flux components for annual estimates in Table 1 and for reference we present the corresponding estimates from the Urban-VPRM. Note that as a light-use efficiency model, the VPRM was developed to capture diurnal and seasonal but not annual trends in CO_2 fluxes.

In the FOREST site inventory soil respiration contributed 72% of the heterotrophic respiration with CWD accounting for the other 28% (Figure 4; Table 1). Leaf respiration dominated the autotrophic respiration flux, comprising 61%. Among the three study plots in the grassland, estimates of NEE varied between −2.74 and −6.77 Mg C ha^{-1} yr^{-1}. Soil respiration represented 44% of grassland Re (Table 1).

GEE estimates in the FOREST site were scaled using seasonal estimates of LAI from either NDVI or SERC observations (see Section 2.2.3 and Figure S5a in Supporting Information S1). The SERC derived LAI scalar consistently yielded slightly higher values of GEE than the NDVI derived LAI scalar except in the fall months when NDVI derived LAI scalar produced slightly higher estimates. Annually, the SERC derived LAI scalar estimated 0.5 more Mg C ha^{-1} yr^{-1} than the SERC approach. We found that the HLS product of land surface phenology significantly overestimated LAI as the canopy senesced, predicting a 50% reduction in LAI when the onsite PhenoCam showed near complete canopy senescence (Figure S5b in Supporting Information S1).

3.2. Comparison Between FOREST Field Inventory and Modeled Estimates

Relative to inventory estimates, the Urban-VPRM closely approximated NEE, however with notable deviations (Figure 5a; Figure 6). In the winter months of November to April, the VPRM overestimated NEE which was driven by overestimate in R_e; the VPRM estimated R_e to be nearly twice as high during these months then was observed in our inventory (Figure 6). In contrast, the VPRM underestimates NEE during spring green-up and fall senescence driven by underestimates in GEE while modeled R_e was in close agreement with inventory observations.

3.3. Comparison Between Modeled Estimates of Forest and Grassland CO_2 Fluxes

A comparison in modeled estimates of seasonal trends in daily mean flux of CO_2 among the forest and grassland areas is show in Figure 5b. Early in the growing season, the uptake of CO_2 is estimated to be higher in the forest than grassland, however, at approximately DOY 210 (mid-August), forest CO_2 uptake declines while grassland CO_2 uptake is maintained. Rates of R_e are four times higher in the forest than the grassland. NEE are similar between the forest and grassland sites with the forest being slightly elevated (or more negative) than the grassland until roughly DOY 210 when the grassland has more negative NEE than the forest site (Figure 5b).

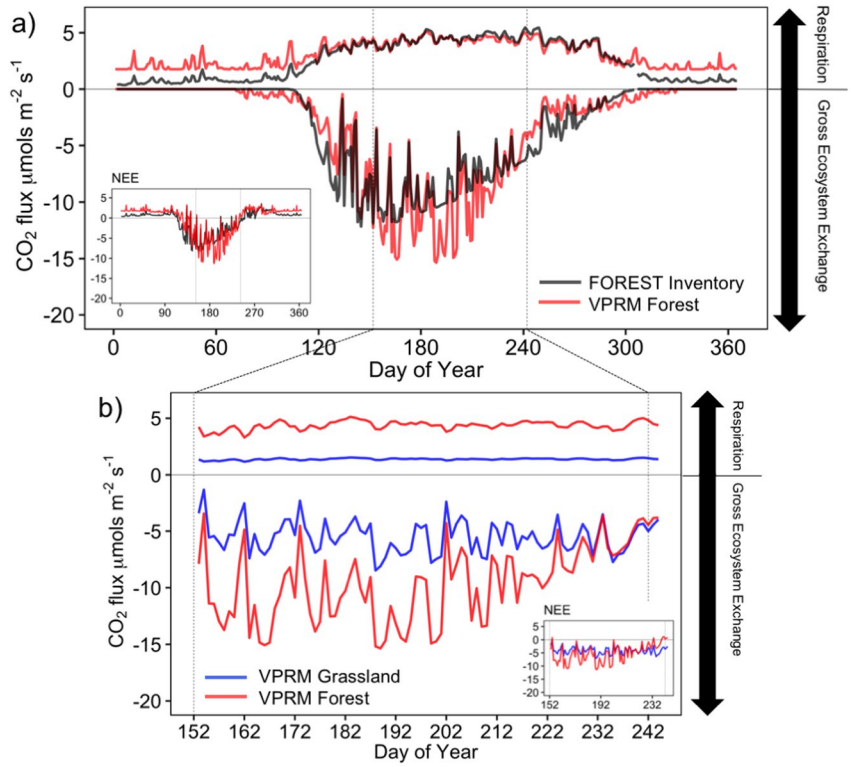

Figure 5. Comparison of carbon fluxes (daily mean, µmols CO_2 m^{-2} s^{-1}) (a) at the Forested Optical Reference for the Evaluation of Sensor Technology (FOREST) site between the field-based inventory (in black) and Urban-Vegetation Photosynthesis and Respiration Model (VPRM; in red), and (b) between the Urban-VPRM runs for the FOREST (in red) and grassland (in blue). Positive values of carbon flux represent ecosystem respiration while negative carbon fluxes represent gross ecosystem exchange of carbon dioxide. Dashed lines represent the months of June to August (DOY 152–243). Panel b shows data from only this time period. In panels (a and b), an inset shows the resulting NEE ($-$GEE + R_e) for each comparison. *Note*. The axis are the same for the inset as the main panel figure.

3.4. Comparison Between VPRM Biogenic Flux Estimates and Anthropogenic Fossil Fuel Emissions

The mean annual flux of FF-CO_2 in our study area ranged from 2.9 µmols FF-CO_2 m^{-2} s^{-1} to 3.3 µmols FF-CO_2 m^{-2} s^{-1} in the ACES pixels that overlap with FOREST study site. In the 6 km^2 area surrounding the FOREST

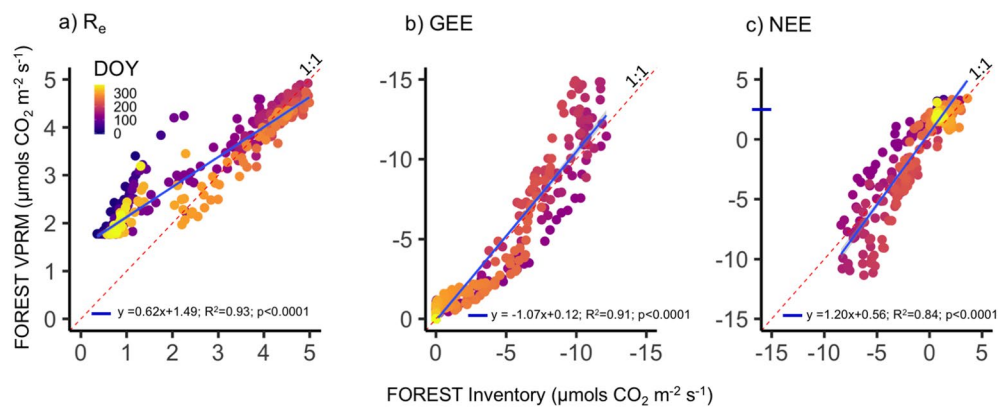

Figure 6. Relationship between Forested Optical Reference for the Evaluation of Sensor Technology (FOREST) Urban-Vegetation Photosynthesis and Respiration Model estimates (*y*-axis) and FOREST field inventory based estimates (*x*-axis) for (a) R_e, (b) gross ecosystem exchange, and (c) net ecosystem exchange. Colors indicate the DOY. The dashed red line is the 1:1 line. The blue line is a linear regression through all points. The equation for the linear regression, R^2, and *p*-value are shown on the bottom of the figure.

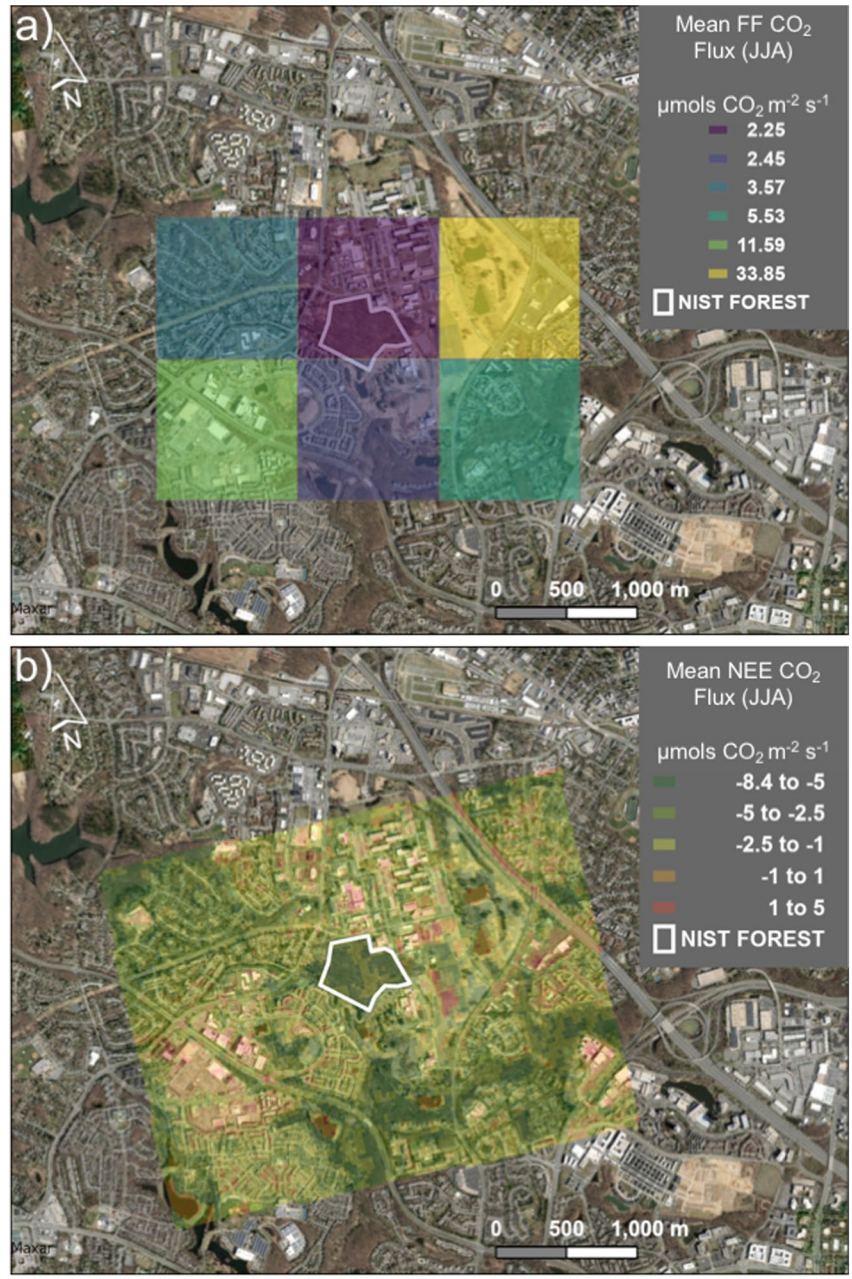

Figure 7. Aerial map showing spatial variability for 6 km^2 area around Forested Optical Reference for the Evaluation of Sensor Technology study site (outlined in white) in mean June through August (June, July, and August) daily estimates of (a) anthropogenic fossil fuel carbon dioxide emissions derived from Anthropogenic Carbon Emissions System inventory (Gately & Hutyra, 2018) and (b) net ecosystem exchange from the Urban-Vegetation Photosynthesis and Respiration Model at a 30 m resolution.

site we observed upwards of 33.6 μmols FF-CO_2 m^{-2} s^{-1} with a mean annual flux of 11.30 μmols FF-CO_2 m^{-2} s^{-1} and mean flux during June through August of 9.87 μmols FF-CO_2 m^{-2} s^{-1} (Figure 7a). There are strong temporal dynamics in FF-CO_2 (Figure 8), with higher emissions in the winter for the 6 km^2 study area (daily mean of 12.39 μmols FF-CO_2 m^{-2} s^{-1}) than during summer months (9.74 μmols FF-CO_2 m^{-2} s^{-1}). The trend in GEE is the opposite; in the summer months there is daily mean of −5.74 μmols CO_2 m^{-2} s^{-1} while in the winter there is no carbon uptake in this deciduous forest. Re has a narrow range across the year ranging from 1.76 μmols CO_2 m^{-2} s^{-1} in the winter to 4.20 μmols CO_2 m^{-2} s^{-1} in the summer. In the summer months, the biogenic CO_2 fluxes in this study area closely approximate FF-CO_2 emissions during the afternoon hours (11:00 to 16:00 local

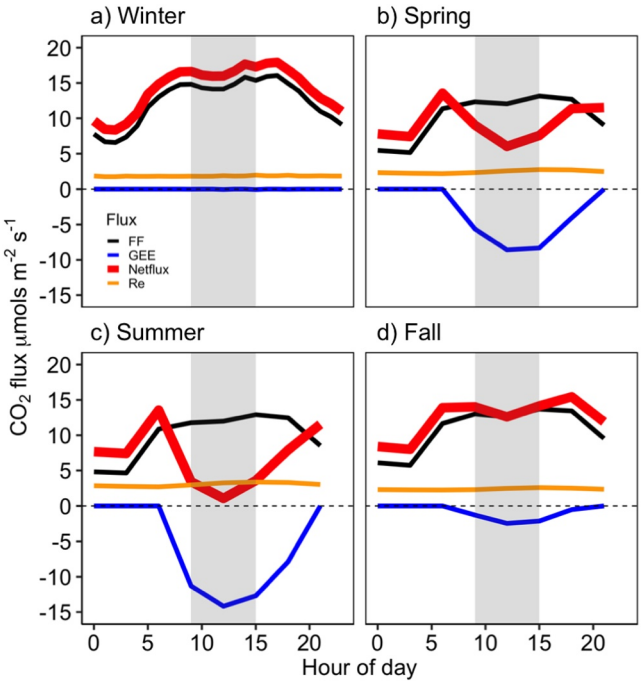

Figure 8. Seasonal variability in mean diurnal trends in CO_2 fluxes from fossil fuels (FF), biogenic gross ecosystem exchange (GEE), biogenic ecosystem respiration (R_e), and the net flux (biogenic + FF) for (a) winter, (b) spring, (c) summer, and (d) fall. FF fluxes are shown in black, GEE is shown in blue, R_e is shown in orange, and net flux is shown as a double red line. The shaded gray region indicates the hours of 11:00 to 16:00 which represent when the atmosphere is turbulent and relatively well-mixed.

time) when the atmosphere is turbulent and relatively well mixed (Sargent et al., 2018) (shown as grayed out time period on Figure 8). During this time period there is a net mean flux of 1.07 µmols CO_2 m^{-2} s^{-1} with net biogenic uptake (-GEE + R_e) representing 91% of the FF-CO_2 flux. Conversely, in the fall and spring the biogenic CO_2 flux (-GEE + R_e) represents 0.08% and 49%, respectively, of the FF-CO_2 emissions during the afternoon hours.

4. Discussion

Cities are taking the lead on climate action with ambitious goals to reduce CO_2 emissions, often proposing nature-based solutions for reaching emission reduction goals (Rosenzweig et al., 2010). However, for cities to develop effective policies and know that they are meeting their goals they need to understand how urbanization influences C cycling dynamics and have accurate CO_2 monitoring systems that can capture the temporal and spatial variability in these CO_2 flux dynamics that occur across cityscapes (Duren & Miller, 2012; Hutyra et al., 2014). Historically, such efforts have largely ignored the contribution of biogenic CO_2 fluxes. Here, we report a detailed carbon inventory, the first of its kind, of the major biologically driven CO_2 fluxes (Figure 1) in an urban forest patch and adjacent unmanaged grassland (Figure 2), illustrating the important role vegetation and soils play in urban C cycling. We compare our inventory estimates to a model-based estimate of biogenic CO_2 fluxes using the Urban-VPRM providing an evaluation of the model in an urban forest patch. In the process we identify key areas for model improvements, in particular the approach used to model urban R_e. Using the Urban-VPRM we compare fine temporal estimate of CO_2 flux dynamics (daily mean) during the growing season in the grassland and forested areas. By placing these biogenic fluxes within the context of total regional fluxes (biogenic and anthropogenic) we demonstrate the seasonal and temporal significance of biogenic fluxes in urban C cycling.

4.1. Characterization of Urban Biogenic Carbon Stocks and CO_2 Fluxes

We find that the urban conditions at the FOREST site have resulted in a productive forest stand and grassland. The forest stores 189.5 Mg C ha^{-1} with a net biogenic carbon uptake of 2.63 ± 1.9 Mg C ha^{-1} yr^{-1} (Table 1; Figure 3). Similar *L. tulipifera/Quercus* sp. dominated forests in the region (within 145 km) have AGB that ranges from 170 to 250 Mg C ha^{-1} (Anderson-Teixeria et al., 2015; Duncanson et al., 2015; Stoval et al., 2018). The observed net productivity of this urban forest persists despite the lack of tree recruitment into canopy gaps (Figure S4b in Supporting Information S1), elevated rates of R_e from both a large pool and flux of CWD, and 16% enhancement in rates of soil respiration due to forest edge effects (Smith, Hutyra, et al., 2019, Table 1). The CWD flux is twice as high as those observed in other well-studied rural forests of northeastern United States (Liu et al., 2006). Additionally, we find the unmanaged grassland to act as a large C sink during the summer months of June through August (−4.86 ± 0.82 Mg C ha^{-1} yr^{-1}) that is similar in magnitude as the net flux of CO_2 observed in the FOREST site (−4.80 ± 0.46 Mg C ha^{-1} yr^{-1}). In the case of the FOREST site, we show that much of this uptake of CO_2 in the summer is respired from the soils in the remaining portion of the year. The growing-season uptake is likely also respired during the remainder of the year in the grasslands, but we do not have direct field data from the grassland for the full year.

Relatively few studies have explicitly compared carbon fluxes in urban forests versus grasslands (Hill et al., 2021; Jo & McPherson, 1995; Parazoo et al., 2021). Typically these studies have been done on grasslands that are receiving higher levels of management (i.e., mowing, fertilizer, and/or irrigation) than observed in this study, as is common in urban areas. The grassland in our study system does not receive any amendments, and perhaps as a consequence, we observed lower grassland R_e fluxes relative to the FOREST site and relative to other studies in urban managed grasses (Hill et al., 2021). Conversely, we observed relatively similar fluxes during the growing season in GEE between the FOREST and grassland (which includes leaf respiration). This trend, however,

changes at DOY 210 when productivity in the forest declines while it is maintained in the grassland resulting in more negative NEE flux in the grassland, at the end of the growing season (Figure 4b). More studies are needed characterizing different vegetation types found in urban/suburban areas (e.g., forest patches vs. street trees vs. grasses) and across different management decisions.

The management decisions made surrounding invasive species, deer populations, and general landscaping practices (e.g., pruning, irrigation, fertilization, mulching, litter removal, replanting practices, etc.) in urban areas have significant impacts on carbon balance of urban areas (Bressette & Beck, 2013; Hundertmark et al., 2021; Parazoo et al., 2021; Pataki et al., 2011; Templer et al., 2015; Townsend-Small & Czimczik, 2010; Winbourne et al., 2020). Our study site, similar to other urban areas in northeastern United States, has high deer densities (30–100 individuals km^{-2}; Rutberg & Naugle, 2008), abundance of invasive plant species (Gaertner et al., 2017), and fragmented forest patches (Morreale et al., 2021; Reinmann et al., 2020). The high deer densities have imposed excessive browsing pressure that limits tree regeneration and facilitates the establishment of unpalatable, but highly productive invasive plant species such as the *M. vimineum* (Averill et al., 2017; Morrison, 2017). The forest floor in our study plot is blanketed with *M. vimineum* (Figure 1) and we observe zero recruitment of saplings during the three-year time period examined with low AGB and stem density in small DBH size trees suggesting this lack of recruitment has been occurring for a longer period than the three-year period examined (Figure 3; Figure S4 in Supporting Information S1). The proliferation of invasive plants in forests of urban landscapes introduces perturbations to forest C balance with few analogs in the minimally disturbed rural systems typically used to inform estimates of regional C balance.

4.2. Comparison Between Inventory and Modeled Estimates of Biogenic CO_2 Fluxes

To develop more accurate predictive models of urban biogenic CO_2 fluxes, our study highlights the need for model improvements on the R_e component of the Urban-VPRM model. Compared to the field estimates, the Urban-VPRM substantially overestimates R_e during the winter months (Piana et al., 2019, Figures 5 and 6). Between the months of November and April the VPRM estimates that R_e is twice as high as our field inventory would suggest. The VPRM simplistically estimates R_e year-round as a piecewise linear function of air temperature with R_e being set to a low, user-defined, constant value during the portion of the year with low air temperatures. Soil respiration, however, is known to be more heavily influence by soil rather than air temperatures especially during the winter months (Grogan & Jonasson, 2006; Morgner et al., 2010). In the Polar-VPRM, R_e estimates were improved by using soil temperature rather than air temperature data (Luus & Lin, 2015). Soil temperature data at higher spatial resolution could help to capture the effects of forest fragmentation on soil respiration that are not currently being captured by the Urban-VPRM (Figure S8 in Supporting Information S1) but is observed in in our inventory estimates (see Smith, Hutyra, et al., 2019). In the case where soil temperature data is not available, an alternative approach to improve VPRM based R_e estimates could include a temporally dynamic parameterization of R_e at a seasonal or monthly timestep rather than current annual approach. Hilton et al. (2013) argues that an ideal model parameter estimation scheme would permit parameter values to vary at space and timescales that match those observed in NEE and illustrates this by finding significant variability in the VPRM parameters for R_e among different months. Additional modifications to the R_e equation have been proposed by Gourdji et al. (2021) in recent modification of the VPRM, including a quadratic temperature term, a vegetation index to capture seasonality in autotrophic respiration, and a water stress scaling factor to capture drought effects on soil moisture conditions.

During the growing season, however, the VPRM closely approximates R_e in the FOREST site which is remarkable given the simplistic nature of the VPRM R_e formulation. In the VPRM, R_e is based on a linear function of air temperature with R_e that is quantified for the Duke Forest AmeriFlux site (US-Dk2) in North Carolina. The VPRM is not designed to capture the unique features of urbanization that influence R_e except for heterotrophic respiration being suppressed by the presence of ISA in urban areas while retaining autotrophic respiration from vegetation overhanging ISA. On the one hand, the close match in VPRM and inventory estimates could suggest that the unique impacts of urbanization on R_e are small compared to temperature driven impacts on R_e. For example, Smith, Hutyra, et al. (2019) observed that forest fragmentation results in a 16% increase in soil respiration rates at the forest edge, however, this edge effect was observed to occur to a distance of 12.5 m from a forest edge which only represents 14% of our FOREST study plot. On the other hand, it is possible that we are obtaining the reasonable answer from the VPRM (i.e., field inventory estimates) for the wrong reasons. For example, the VPRM is not intended to capture the large CO_2 flux from CWD pool that we observe at our field site. The VPRM

is parameterized based on CWD flux dynamics observed at the Duke Forest AmeriFlux site (US-Dk2) in North Carolina which has a much smaller CWD pool than is observed at our site. Consequently, the VPRM may be obtaining the same R_e that we observe in our field inventory by underestimating CWD flux and overestimating autotrophic and other components of the heterotrophic respiration flux. Collectively, this highlights the need for more CO_2 flux inventories in urban areas across different land use types to determine the applicability of the Urban-VPRM for capturing urban R_e dynamics.

In contrast, the Urban-VPRM closely approximates estimates of GEE (Figures 5 and 6). This is perhaps not surprising given both approaches have in common a focus on light-use efficiency. In the case of the VPRM this light-use efficiency model is parameterized with eddy covariance data (Mahadevan et al., 2008) while in the inventory estimates we used LRC measurements from our field site to scale measurements at the leaf-level to the entire canopy. While the big-leaf modeling approach is commonly used in land surface models (Sprintsin et al., 2012), to our knowledge, our study represents the first time this approach has been applied to an urban forest.

The big-leaf modeling and eddy covariance approaches for estimating GEE have known challenges especially in urban landscapes. The big-leaf model assumptions do not capture the complex structures of canopies (e.g., leaf distribution varies by clumping, light environments, leaf angles, and canopy heights) and consequently have been found to underestimate GEE (Friend, 2001; Luo et al., 2018). Eddy covariance methodologies are often challenging to use in urban areas with heterogenous land cover, which confounds partitioning fluxes (Grimmond et al., 2002). The strong coupling between transpiration (or movement of tree sap) and photosynthesis suggests that the quantification of tree-level sap flux as an alternative method for obtaining temporal and spatially refined estimates of canopy level carbon assimilation (Schäfer et al., 2003). Recent advancements in sap flux sensor technology (Jones et al., 2020) now allows for the creation of relatively large networks needed to generate robust estimates of GEE in urban vegetation.

There are small, but notable differences in temporal trends between the GEE VPRM and inventory estimates (Figures 5 and 6). For example, in the shoulder seasons (spring green-up and fall senescence) the VPRM predicts earlier green up (higher GEE) and later senescence (lower GEE) than the inventory approach. The mismatch between the VPRM and inventory estimates of GEE could be in part due to our LAI proxy not representing the true LAI at our field site. LAI is known to be a dominant control over primary production (Asner et al., 2003; Parker, 2020) and important source of error in big-leaf modeling approaches used to scale leaf-level measurements of photosynthesis (Richardson et al., 2012). Unfortunately, PhenoCam derived measures of greenness do not provide accurate estimates of LAI and while NDVI or EVI derived LAI estimates are found as relatively good proxies of empirically measured LAI, these approaches are relatively insensitive to changes in LAI at high levels (>2) observed at our FOREST site that introduce errors in estimates of vegetation productivity (Keenan et al., 2014).

4.3. Comparison Between Modeled Biogenic Fluxes and Anthropogenic Fossil Fuel Emissions

Using the Urban-VPRM, we expanded the spatial scope of our analysis to a 6 km^2 area around the FOREST site and evaluated in this area when and where net biogenic CO_2 fluxes begin to significantly influence the net (i.e., biogenic + FF) CO_2 flux signal. The ACES emissions inventory (Gately & Hutyra, 2017, 2018) provides detailed sectoral, temporal, and spatial resolution of FF-CO_2 emissions highlighting that local FF emissions are dominated by on-road sources (Figure 7a) with diurnal peaks in emissions occurring during traditional commuting hours of early morning and evening (Figure 8).

Our study adds to a growing body of literature illustrating the importance of including biogenic sources of CO_2 when generating estimates of CO_2 fluxes in urban areas at fine spatial and temporal resolutions (Miles et al., 2021; Sargent et al., 2018). Similar to the top-down study by Sargent et al. (2018), we observed seasonal trends in the magnitude of biogenic CO_2 fluxes when examine the VPRM run for a 6 km^2 area around our FOREST site. These findings have implications on identifying when and where accurate estimates of biogenic fluxes are most important for understanding urban C cycling and identifying the extent to which biology can help offset CO_2 emissions from FF sources (Figures 7 and 8). For example, in our spatial analysis of biogenic CO_2 fluxes in our 6 km^2 study region (Figure 7b) we observe areas with high ISA being a net source of biogenic CO_2 (−1 to −5 μmol CO_2 m^{-2} s^{-1}) and areas dominated by vegetation varying in the extent to which they are a net sink of CO_2 (0 to −8.4 μmol CO_2 m^{-2} s^{-1}). Spatial variability in net CO_2 uptake by vegetation and soils highlights the differences in urban vegetation structure and function across the landscape with higher CO_2 uptake in forest

patches than in grassland or street tree dominated areas (Figure 7b). While FF emissions dominate the net flux signal in the study region both at diurnal and annual scales, resulting in the region being a net source of CO_2, we identify key time periods when high rates of CO_2 uptake by vegetation can nearly match those of FF-CO_2 emissions. During the summer afternoons (the hours of 11:00 to 16:00) when air is turbulent and well mixed, we find net biogenic CO_2 fluxes to represent 91% of the FF-CO_2 flux. In contrast, during the winter months when vegetation is not photosynthesizing and soil respiration rates are low, the net biogenic flux only accounted for 0.08% of the FF-CO_2 flux (Figure 8). The daytime aliasing of FF-CO_2 emissions due to biological uptake poses a substantial challenge in the application of atmospheric inversions for carbon monitoring. Our study highlights the importance of including seasonal dynamics in biogenic CO_2 fluxes when planning and testing efficacy of greenhouse gas emission reduction polices, and identifies the Urban-VPRM as a powerful tool for generating city-wide and regional scale estimates of biogenic C fluxes.

5. Conclusion

We show that the unique conditions of urban areas resulted in temporal and spatial patterns in sink and source dynamics of biogenic fluxes of CO_2 that need to be considered when generating CO_2 monitoring systems and considering nature-based climate solutions. We find in our field measurements that urban vegetation can act as a carbon sink with the forest patch in our study storing 2.62 ± 1.9 Mg C ha^{-1} yr^{-1}. We identify urban vegetation having a strong effect on the signal of the net flux of CO_2 (biogenic + FF) during summertime afternoons. While FF emissions drive patterns in net fluxes at the daily and annual timescale throughout the year, during summer afternoons urban vegetation temporarily takes up roughly the same amount of CO_2 that is being released by FF sources. We find that the VPRM based modeling approach closely approximates inventory observations of GEE, but overestimates R_e in the winter months highlighting key areas for model improvement to generate more accurate estimates of urban NEE. The observed model performance relative to the inventory estimates coupled with the relative ease of use of the Urban-VPRM (e.g., low number of site-specific parameters and relatively widely available remote sensing and meteorological input data) suggests the Urban-VPRM could be a valuable tool for policymakers, NGOs, and researchers that are planning, measuring, and reporting CO_2 fluxes in urban areas.

Conflict of Interest

The authors declare no conflicts of interest relevant to this study.

Data Availability Statement

Data reported in this paper are available at Dataverse (https://doi.org/10.7910/DVN/UNF7EB and https://doi.org/10.7910/DVN/ZLRKK2 created for Smith, Dearborn, & Hutyra, 2019). Certain commercial equipment, instruments, or materials (suppliers or software) are identified in this paper to foster understanding. Such identification does not imply recommendation or endorsement by the National Institute of Standards and Technology nor does it imply that the materials or equipment identified are necessarily the best available for the purpose.

Acknowledgments
This work was supported by the National Institute of Standards and Technology Award 70NANB17H030. The authors thank James Whetstone, Sharon Gourdji, Taylor S. Jones, Julia Marrs, Wiley Hundertmark, Andrew Trlica, and Lauren Cabrera for critical discussion as well as field and laboratory support on this effort. The authors thank an anonymous reviewer for their helpful comments.

References

Ainsworth, E. A., Yendrek, C. R., Sitch, S., Collins, W. J., & Emberson, L. D. (2012). The effects of tropospheric ozone on net primary productivity and implications for climate change. *Annual Review of Plant Biology*, *63*, 637–661. https://doi.org/10.1146/annurev-arplant-042110-103829

Anderson-Teixeria, K. J., McGarvey, J. C., Muller-Landau, H. C., Park, J. Y., Gonzalez-Akre, E. B., Hermann, V., et al. (2015). Size-related scaling of tree form and function in a mixed-age forest. *Functional Ecology*, *29*(12), 1587–1602. https://doi.org/10.1111/1365-2435.1240

Asner, G. P., Scurlock, J. M. O., & Hicke, J. A. (2003). Global synthesis of leaf area index observations: Implications for ecological and remote sensing studies. *Global Ecology and Biogeography*, *12*(3), 191–205. https://doi.org/10.1046/j.1466-822x.2003.00026.x

Averill, K. M., Mortensen, D. A., Smithwick, E. A. H., Kalisz, S., McShea, W. J., Bourg, N. A., et al. (2017). A regional assessment of white-tailed deer effects on plant invasion. *AoB PLANTS*, *10*, plx047. https://doi.org/10.1093/aobpla/plx047

Benjamin, S. G., Weygandt, S. S., Brown, J. M., Hu, M., Alexander, C. R., Smirnova, T. G., et al. (2016). A North American hourly assimilation and model forecast cycle: The Rapid Refresh. *Monthly Weather Review*, *144*(4), 1669–1694. https://doi.org/10.1175/MWR-D-15-0242.1

Bergeron, O., & Strachan, I. B. (2011). CO_2 sources and sinks in urban and suburban areas of a northern mid-latitude city. *Atmospheric Environment*, *45*, 1564–1573. https://doi.org/10.1016/j.atmosenv.2010.12.043

Boesch, H., Baker, D., Connor, B., Crisp, D., & Miller, C. (2011). Global characterization of CO_2 column retrievals from shortwave-infrared satellite observations of the orbiting carbon observatory-2 mission. *Remote Sensing*, *3*(2), 270–304. https://doi.org/10.3390/rs3020270

Bolton, D. K., Gray, J. M., Melaas, E. K., Moon, M., Eklundh, L., & Friedl, M. A. (2020). Continental-scale land surface phenology from harmonized Landsat 8 and Sentinel-2 imagery. *Remote Sensing of Environment*, *240*, 111685. https://doi.org/10.1016/j.rse.2020.111685

Bressette, J. W., & Beck, H. (2013). The effects of high deer density on forest regeneration and carbon sequestration. *Environmental Research*, *7*(1), 436–4140

Briber, B., Hutyra, L. R., Reinmann, A. B., Raciti, S. M., Dearborn, V. K., Holdern, C. E., & Dunn, A. L. (2015). Tree productivity enhanced with conversion from forest to urban land covers. *PLoS One*, *10*(8), e0136237. https://doi.org/10.1371/journal.pone.0136237

Chen, S., Chen, B., Feng, K., Liu, Z., Fromer, N., Tan, X., et al. (2020). Physical and virtual carbon metabolism of global cities. *Nature Communications*, *11*, 182. https://doi.org/10.1038/s41467-019-13757-3

Chojnacky, D. C., Heath, L. S., & Jenkins, J. C. (2014). Updated generalized biomass equations for North American tree species. *Forestry: International Journal of Financial Research*, *87*(1), 129–151. https://doi.org/10.1093/forestry/cpt053

Churkina, G. (2008). Modeling the carbon cycle of urban systems. *Ecological Modeling*, *216*(2), 107–113. https://doi.org/10.1016/j.ecolmodel.2008.03.006

Churkina, G. (2016). The role of urbanization in the global carbon cycle. *Frontiers in Ecology and Evolution*, *3*(144), 1–9. https://doi.org/10.3389/fevo.2015.00144

Churkina, G., Brown, D. G., & Keoleian, G. (2010). Carbon stored in human settlements: The conterminous United States. *Global Change Biology*, *16*, 135–143. https://doi.org/10.1111/j.1365-2486.2009.02002.x

Clark, D. A., Brown, S., Kicklighter, D. W., Chamber, J. Q., Thomlinson, J. R., & Ni, J. (2001). Measuring net primary production in forests: Concepts and field methods. *Ecological Applications*, *11*(2), 356–370. https://doi.org/10.1890/1051-0761(2001)011[0356:mnppif]2.0.co;2

Claverie, M., Ju, J., Masek, J. G., Dungan, J. L., Vermote, E. F., Roger, J., et al. (2018). The Harmonized Landsat and Sentinel-2 surface reflectance data set. *Remote Sensing of Environment*, *219*, 145–161. https://doi.org/10.1016/j.rse.2018.09.002

Crawford, B., Grimmond, C. S. B., & Christen, A. (2011). Five years of carbon dioxide fluxes measurements in a highly vegetated suburban area. *Atmospheric Environment*, *45*, 896–905. https://doi.org/10.1016/j.atmosenv.2010.11.017

Crockatt, M. E., & Bebber, D. P. (2015). Edge effects on moisture reduce wood decomposition rate in a temperate forest. *Global Change Biology*, *21*, 698–707. https://doi.org/10.1111/gcb.12676

Davidson, E. A., Belk, E., & Boone, R. D. (1998). Soil water content and temperature as independent or confounded factors controlling soil respiration in a temperate mixed hardwood forest. *Global Change Biology*, *4*(2), 217–227. https://doi.org/10.1046/j.1365-2486.1998.00128.x

Decina, S. M., Hutyra, L. R., Gately, C. K., Getson, J. M., Reinmann, A. B., Short Gianotti, A. G., & Templer, P. H. (2016). Soil respiration contributes substantially to urban carbon fluxes in the greater Boston area. *Environmental Pollution*, *212*, 433–439. https://doi.org/10.1016/j.envpol.2016.01.012

Duncanson, L. I., Dubayah, R. O., Cook, B. D., Rosette, J., & Parker, G. (2015). The importance of spatial detail: Assessing the utility of individual crown information and scaling approaches for lidar-based biomass density estimation. *Remote Sensing of Environment*, *168*, 102–112. https://doi.org/10.1016/j.rse.2015.06.021

Duren, R. M., & Miller, C. E. (2012). Measuring the carbon emissions of megacities. *Nature Climate Change*, *2*, 560–562. https://doi.org/10.1038/nclimate1629

EUMETSAT OSI SAF. (2018). Geostationary radiation fluxes product user manual. Retrieved from https://osi-saf.eumetsat.int/lml/doc/osisaf_cdop3_ss1_pum_geo_flx.pdf

EUMETSAT OSI SAF. (2021). Geostationary radiative fluxes: GOES-E surface solar irradiance product OSI-305-b. Retrieved from https://osi-saf.eumestsat.int/products/osi-306-b

Fahey, T. J., Siccama, T. G., Driscoll, C. T., Likens, G. E., Campbell, J., Johnson, C. E., et al. (2005). The biogeochemistry of carbon at Hubbard Brook. *Biogeochemistry*, *75*, 109–176. https://doi.org/10.1007/s10533-004-6321-y

Fargione, J. E., Bassett, S., Boucher, T., Bridgham, S. D., Conant, R. T., Cook-Patton, S. C., et al. (2018). Natural climate solutions for the United States. *Science Advances*, *4*, eaat1869.

Frazer, G. W., Canham, C. D., & Lertzman, K. P. (1999). *Gap Light Analyzer (GLA), version 2.0: Imaging software to extract canopy structure and gap light transmission indices from true-colour fisheye photographs, user manual and program documentation*. Simon Fraser Univerity, Burnaby, British Columbia, and the Institute of Ecosystem Studies, Millbrook.

Friend, A. D. (2001). Modeling canopy CO_2 fluxes: Are 'Big-Leaf' simplifications justified? *Global Ecology and Biogeography*, *10*(6), 603–619. https://doi.org/10.1046/j.1466-822x.2001.00268.x

Gaertner, M., Wilson, J. R. U., Cadotte, M. W., Maclvor, J. S., Zenni, R. D., & Richardson, D. M. (2017). Non-native species in urban environments: Patterns, processes, impacts and challenges. *Biological Invasions*, *19*, 3461–3469. https://doi.org/10.1007/s10530-017-1598-7

Gately, C., & Hutyra, L. R. (2017). Large uncertainties in urban-scale carbon emissions. *Journal of Geophysical Research: Atmospheres*, *122*(11), 11242–11260. https://doi.org/10.1002/2017jd027359

Gately, C., & Hutyra, L. R. (2018). *CMS: CO_2 emissions from fossil fuels combustion, ACES inventory for Northeastern USA*. ORNL DAAC. https://doi.org/10.3334/ORNLDAAC/1501

Gately, C., Hutyra, L. R., & Wing, I. S. (2015). Cities, traffic, and CO_2: A multidecadal assessment of trends, drivers, and scaling relationships. *Proceedings of the National Academy of Sciences*, *112*(16), 4999–5004. https://doi.org/10.1073/pnas.1421723112

Giasson, M. A., Ellison, A. M., Bowden, R. D., Crill, P. M., Davidson, E. A., Drake, J. E., et al. (2013). Soil respiration in a northeastern US temperate forest: A 22-year synthesis. *Ecosphere*, *4*(11), 140. https://doi.org/10.1890/ES13.00183.1

Golubiewski, N. E. (2006). Urbanization increases grassland carbon pools: Effects of landscaping in Colorado front range. *Ecological Applications*, *16*, 555–571. https://doi.org/10.1890/1051-0761(2006)016[0555:uigcpe]2.0.co;2

Gough, C. M., & Elliott, H. L. (2012). Lawn soil carbon storage in abandoned residential properties: An examination of ecosystem structure and function following partial human-natural decoupling. *Journal of Environmental Management*, *98*, 155–162. https://doi.org/10.1016/j.jenvman.2011.12.028

Gourdji, S. M., Karion, A., Lopez-Coto, I., Ghosh, S., Mueller, K., Zhou, Y., et al. (2021). A modified Vegetation Photosynthesis and Respiration Model (VPRM) for the eastern USA and Canada, evaluated with comparison to atmospheric observations and other biospheric models. *Journal of Geophysical Research: Biogeosciences*. https://doi.org/10.1002/essoar.10506768.1

Grimmond, C. S. B., King, T. S., Cropley, F. D., Nowak, D. J., & Souch, C. (2002). Local-scale fluxes of carbon dioxide in urban environments: Methodological challenges and results from Chicago. *Environmental Pollution*, *116*. https://doi.org/10.1016/s0269-7491(01)00256-1

Grogan, P., & Jonasson, S. (2006). Ecosystem CO_2 production during winter in a Swedish subarctic region: The relative importance of climate and vegetation type. *Global Change Biology*, *12*, 1479–1495. https://doi.org/10.1111/j.1365-2486.2006.01184.x

Gu, Y., Hunt, E., Wardlow, B., Basara, J. B., Brown, J. F., & Verdin, J. P. (2008). Evaluation of MODIS NDVI and DNWI for vegetation drought monitoring using Oklahoma Mesonet soil moisture data. *Geophysical Research Letters*, *35*, L22401. https://doi.org/10.1029/2008gl035772

Gurney, K. R., Chen, Y. H., Maki, T., Kawa, S. R., Andrews, A., & Zhu, Z. (2005). Sensitivity of atmospheric CO_2 inversion to seasonal and interannual variations in fossil fuel emissions. *Journal of Geophysical Research*, *110*(D10), 10308–10321. https://doi.org/10.1029/2004jd005373

Hanson, P. J., Edwards, N. T., Garten, C. T., & Andrews, J. A. (2000). Separating root and soil microbial contributions to soil respiration: A review of methods and observations. *Biogeochemistry*, *48*, 115–146. https://doi.org/10.1023/a:1006244819642

Hardiman, B., Wang, J., Hutyra, L. R., Gately, C., Getson, J., & Friedl, M. (2017). Accounting for urban biogenic fluxes in regional carbon budgets. *The Science of the Total Environment*, *592*, 366–372. https://doi.org/10.1016/j.scitotenv.2017.03.028

Haynes, K. D., Baker, I. T., Denning, A. S., Stöckli, R., Schaefer, K., Lokupitiya, E. Y., & Haynes, J. M. (2019). Representing grasslands using dynamic prognostic phenology based on biological growth stages: 1. Implementation in the simple biosphere model (SiB3). *Journal of Advances in Modeling Earth Systems*, *11*(12), 4423–4439. https://doi.org/10.1029/2018ms001540

Helfter, C., Famulari, D., Phillips, G. J., Barlow, J. F., Wood, C. R., Grimmond, C. S. B., & Nemitz, E. (2011). Controls of carbon dioxide concentrations and fluxes above central London. *Atmospheric Chemistry and Physics*, *11*, 1913–1928. https://doi.org/10.5194/acp-11-1913-2011

Hill, A., Barba, J., Hom, J., & Vargas, R. (2021). Patterns and drivers of multi-annual CO_2 emissions within a temperate suburban neighborhood. *Biogeochemistry*, *152*, 35–50. https://doi.org/10.1007/s10533-020-00731-1

Hilton, T. W., Davis, K. J., & Keller, K. (2014). Evaluating terrestrial CO_2 flux diagnoses and uncertainties from a simple land surface model and its residuals. *Biogeosciences*, *11*, 217–235. https://doi.org/10.5194/bg-11-217-2014

Hilton, T. W., Davis, K. J., Keller, K., & Urban, N. M. (2013). Improving North American terrestrial CO_2 flux diagnosis using spatial structure in land surface model residuals. *Biogeosciences*, *10*, 4607–4625. https://doi.org/10.5194/bg-10-4607-2013

Homer, C. G., Dewitz, J. A., Yang, L., Jin, S., Danielson, P., Xian, G., et al. (2015). Completion of the 2011 National Land Cover Database for the conterminous United States – Representing a decade of land cover change information. *Photogrammetric Engineering & Remote Sensing*, *81*, 345–354

Hsu, A., Höhne, N., Kuramochi, T., Roelfsema, M., Weinfurter, A., Xie, Y., et al. (2019). A research roadmap for quantifying non-state and subnational climate mitigation action. *Nature Climate Change*, *9*, 11–17. https://doi.org/10.1038/s41558-018-0338-z

Hundertmark, W. J., Lee, M., Smith, I. A., Bang, A. H. Y., Chen, V., Gately, C. K., et al. (2021). Influence of landscape management practices on urban greenhouse gas budgets. *Carbon Balance and Management*, *16*(1), 1–12. https://doi.org/10.1186/s13021-020-00160-5

Hutchison, J. S., & Henry, H. A. L. (2010). Additive effects of warming and increased nitrogen deposition in a temperate old field: Plant productivity and the importance of winter. *Ecosystems*, *13*(5), 661–672. https://doi.org/10.1007/s10021-010-9344-3

Hutyra, L. R., Duren, R., Gurney, K., Grimm, N., Kort, E., Larson, E., & Shrestha, G. (2014). Urbanization and the carbon cycle: Current capabilities and research outlook from the natural sciences perspective. *Earth Future*, *2*(10), 473e495. https://doi.org/10.1002/2014ef000255

Ives, C. D., Lentini, P. E., Threlfall, C. G., Ikin, K., Shanahan, D. F., Garrad, G. E., et al. (2016). Cities are hotspots for threatened species. *Global Ecology and Biography*, *25*, 117–126. https://doi.org/10.1111/geb.12404

Järvi, L., Nordbo, A., Junninen, H., Riikonen, A., Moilanen, J., Nikinmaa, E., & Vesala, T. (2012). Seasonal and annual variation of carbon dioxide surface fluxes in Helsinki, Finland. *Atmospheric Chemistry and Physics*, *12*, 8475–8489

Jo, H.-K. (2002). Impacts of urban greenspace on offsetting carbon emissions for middle Korea. *Journal of Environmental Management*, *64*, 115–126. https://doi.org/10.1006/jema.2001.0491

Jo, H.-K., & McPherson, G. (1995). Carbon storage and flux in urban residential greenspace. *Journal of Environmental Management*, *45*, 109–133. https://doi.org/10.1006/jema.1995.0062

Jones, T. S., Winbourne, J. B., & Hutyra, L. R. (2020). Ribbonized sap flow: An emerging technology for the integration of sap flow sensor components onto a single platform. *Ecosphere*, *11*(6), e03135. https://doi.org/10.1002/ecs2.3135

Kaye, J. P., McCulley, R. L., & Burke, I. C. (2005). Carbon fluxes, nitrogen cycling, and soil microbial communities in adjacent urban, native, and agricultural ecosystems. *Global Change Biology*, *11*(4), 575–587. https://doi.org/10.1111/j.1365-2486.2005.00921.x

Keenan, T. F., Darby, B., Felts, E., Sonnentag, O., Friedl, M. A., Hufkens, K., et al. (2014). Tracking forest phenology and seasonal physiology using digital repeat photography: A critical assessment. *Ecological Applications*, *24*(6), 1478–1489. https://doi.org/10.1890/13-0652.1

Kennedy, C., Baker, L., Dhakal, S., & Ramaswami, A. (2012). Sustainable urban systems. *Journal of Industrial Ecology*, *16*(6), 775–779. https://doi.org/10.1111/j.1530-9290.2012.00564.x

Kennedy, C., Steinberger, J., Gasson, B., Hansen, Y., Hillman, T., Havránek, M., et al. (2009). Greenhouse gas emissions from global cities. *Environmental Science & Technology*, *43*, 7297–7302. https://doi.org/10.1021/es900213p

Kim, H. H. (1992). Urban heat island. *International Journal of Remote Sensing*, *13*, 2319–2336. https://doi.org/10.1080/01431169208904271

Kordowski, K., & Kuttler, W. (2010). Carbon dioxide fluxes over an urban park area. *Atmospheric Environment*, *44*(23), 2722e2730. https://doi.org/10.1016/j.atmosenv.2010.04.039

Krupa, S. V., & Manning, W. J. (1988). Atmospheric ozone: Formation and effects on vegetation. *Environmental Pollution*, *50*, 101–137. https://doi.org/10.1016/0269-7491(88)90187-x

Kühn, I., Brandl, R., & Klotz, S. (2004). The flora of German cities is naturally species rich. *Evolutionary Ecology Research*, *6*, 749–764.

Lamb, W. F., Creutzig, F., Callaghan, M. W., & Minx, J. C. (2019). Learning about urban climate solutions from case studies. *Nature Climate Change*, *9*, 1–10. https://doi.org/10.1038/s41558-019-0440-x

Lambers, H., Chapin, F. S., III, & Pons, T. L. (2008). *Plant physiological ecology*. Springer-Verlag. https://doi.org/10.1007/978-0-387-78341-3

Lauvaux, T., Gurney, K. R., Miles, N. L., Davis, K. J., Richardson, S. J., Deng, A., et al. (2020). Policy-relevant assessment of urban CO_2 emissions. *Environmental Science and Technology*, *54*, 10237–10245. https://doi.org/10.1021/acs.est.0c00343

Lavalle, C., & Martins, P. (2002). *Towards an urban atlas: Assessment of spatial data on 25 European cities and urban areas*. European Environmental Agency.

Le Quéré, C., Andres, R. J., Boden, T., Conway, T., Houghton, R. A., House, J. I., et al. (2013). The global carbon budget 1959–2011. *Earth System Science Data*, *5*, 165–185. https://doi.org/10.5194/essd-5-165-2013

Li, D., & Bou-Zeid, E. (2013). Synergistic interactions between urban heat islands and heat waves: The impact in cities is larger than the sum of its parts. *Journal of Applied Meteorology and Climatology*, *52*, 2051–2064. https://doi.org/10.1175/jamc-d-13-02.1

Lin, J., Pejam, M., Chan, E., Wofsy, S., Gottlieb, E., Margolis, H., & McCaughey, J. (2011). Attributing uncertainties in simulated biospheric carbon fluxes to different error sources. *Global Biogeochemical Cycles*, *25*, GB2018. https://doi.org/10.1029/2010GB003884

Liu, W. H., Bryant, D. M., Hutyra, L. R., Saleska, S. R., Hammond-Pyle, E., Curran, D., & Wofsy, S. C. (2006). Woody debris contribution to the carbon budget of selectively logged and maturing mid-latitude forests. *Oecologia*, *148*, 108–117. https://doi.org/10.1007/s00442-006-0356-9

Luo, X., Chen, J. M., Liu, J., Black, T. A., croft, H., Staebler, R., et al. (2018). Comparison of big-leaf, two-big-leaf, and two-leaf upscaling schemes for evapotranspiration estimation using coupled carbon-water modeling. *Journal of Geophysical Research: Biogeosciences*, *123*, 207–225. https://doi.org/10.1002/2017JG003978

Luus, K. A., & Lin, J. C. (2015). The polar vegetation photosynthesis and respiration model: A parsimonious, satellite-data-driven model of high-latitude CO_2 exchange. *Geoscientific Model Development*, *8*, 2655–2674. https://doi.org/10.5194/gmd-8-2655-2015

Luyssaert, S., Inglima, I., Jung, M., Richardson, A. D., Reichstein, M., & Papale, D. (2007). CO_2 balance of boreal, temperate, and tropical forests derived from a global database. *Global Change Biology*, *13*, 2509–2537. https://doi.org/10.1111/j.1365-2486.2007.01439.x

Mahadevan, P., Wofsy, S. C., Matross, D. M., Xiao, X., Dunn, A. L., Lin, J. C., et al. (2008). A satellite-based biosphere parameterization for net ecosystem CO_2 exchange: Vegetation Photosynthesis and Respiration Model (VPRM). *Global Biogeochemical Cycles*, *22*, 1–17. https://doi.org/10.1029/2006gb002735

Maki, M., Krayenhoff, E. S., & Nazarian, N. (2004). Estimation of leaf water status to monitor the risk of forest fires by using remotely sensed data. *Remote Sensing of Environment*, *90*, 441–450. https://doi.org/10.1016/j.rse.2004.02.002

Martin, J., Kloeppel, B. D., Schaefer, T. L., Kimbier, D. L., & McNulty, S. G. (1998). Aboveground biomass and nitrogen allocation of ten deciduous southern Appalachian tree species. *Canadian Journal of Forest Research*, *28*, 1648–1659. https://doi.org/10.1139/x98-146

Masek, J. G., Vermote, E. F., Saleous, N. E., Wolfe, R., Hall, F. G., Huemmrich, K. F., et al. (2006). A Landsat surface reflectance dataset for North America, 1990–2000. *IEEE Geoscience and Remote Sensing Letters*, *3*(1), 68–72. https://doi.org/10.1109/LGRS.2005.857030

McRae, J. E., & Graedel, T. E. (1979). Carbon dioxide in the urban atmosphere: Dependencies and trends. *Journal of Geophysical Research*, *84*(C8), 5011e5017. https://doi.org/10.1029/JC084iC08p05011

Melaas, E. K., Friedl, M. A., & Richardson, A. D. (2016). Multi-scale modeling of spring phenology across deciduous forests in the eastern United States. *Global Change Biology*, *22*, 792–805. https://doi.org/10.1111/gcb.13122

Melaas, E. K., Wang, J. A., Miller, D. L., & Friedl, M. A. (2016). Interactions between urban vegetation and surface urban heat islands: A case study in the Boston metropolitan region. *Environmental Research Letters*, *11*, 54020. https://doi.org/10.1088/1748-9326/11/5/054020

Miles, N., Davis, K. J., Richardson, S. J., Lauvaux, T., Martins, D. K., Deng, A. J., et al. (2021). The influence of near-field fluxes on seasonal carbon dioxide enhancements: Results from the Indianapolis flux experiment (INFLUX). *Carbon Balance and Management*, *16*(4), 1–15. https://doi.org/10.1186/s13021-020-00166-z

Miller, J. B., Lehamn, S. J., Montzka, S. A., Sweeney, C., Miller, B. R., Karion, A., et al. (2012). Linking emissions of fossil fuel CO_2 and other anthropogenic trace gases using atmospheric $^{14}CO_2$. *Journal of Geophysical Research*, *117*(D8), D08302. https://doi.org/10.1029/2011JD017048

Milnar, M., & Ramaswami, A. (2020). Impact of Urban expansion and in situ greenery on community-wide carbon emissions: Method development and insights from 11 US cities. *Environmental Science and Technology*, *54*, 16086–16096. https://doi.org/10.1021/acs.est.0c02723

Morgner, E., Elberling, B., Strebel, D., & Cooper, E. (2010). The importance of winter in annual ecosystem respiration in the high Arctic: Effects of snow depth in two vegetation types. *Polar Research*, *29*, 58–74. https://doi.org/10.1111/j.1751-8369.2010.00151.x

Morreale, L. L., Thompson, J. R., Tang, X., Reinmann, A. B., & Hutyra, L. R. (2021). Elevated growth and biomass along temperate forest edges. *Nature Communications*, *12*, 7181. https://doi.org/10.1038/s41467-021-27373-7

Morrison, J. A. (2017). Effects of white-tailed deer and invasive plants on the herb layer of suburban forests. *AoB PLANTS*, *9*, plx058. https://doi.org/10.1093/aobpla/plx058

National Climatic Data Center. (2018). *Climate data online: Data tools*. Retrieved from www.ncdc.noaa.gov/cdo-web/datatools/normals

Natural Resources Conservation Service. (2018). *Web soil survey*. Retrieved from www.websoilsurvey.sc.egov.usda.gov/App/HomePage.htm

NEON (National Ecological Observatory Network). (2020). *Digital hemispheric photos of plot vegetation, RELEASE-2021 (DP1.10017.001)* (Dataset). https://doi.org/10.48443/crh2-jr84. Retrieved from https://data.neonscience.org

Nowak, D. J. (1993). Atmospheric carbon-reduction by urban trees. *Journal of Environmental Management*, *37*, 207–217. https://doi.org/10.1006/jema.1993.1017

Nowak, D. J. (2020). *Understanidng i-Tree: Summary of programs and methods* (General technical report NRS-200, p. 100). U.S. Department of Agriculture, Forest Service, Northern Research Station.

Nowak, D. J., & Crane, D. E. (2002). Carbon storage and sequestration by urban trees in the USA. *Environmental Pollution*, *116*, 381–389. https://doi.org/10.1016/s0269-7491(01)00214-7

Nowak, D. J., Noble, M. H., Sisinni, S. M., & Dwyer, J. F. (2001). Assessing the US urban forest resource. *Journal of Forestry*, *99*, 37–42

Oishi, C., Novick, K., & Stoy, P. (2018). *AmeriFlux US-Dk2 Duke forest-hardwoods, ver. 4-5, AmeriFlux AMP* (Dataset). https://doi.org/10.17190/AMF/1246047

Oke, T. R. (1982). The energetic basis of the urban heat island. *Quarterly Journal of the Royal Meteorological Society*, *108*, 1–24. https://doi.org/10.1002/qj.49710845502

Ollinger, S. V., Aber, J., & Reich, P. B. (2002). Interactive effects of nitrogen deposition, tropospheric ozone, elevated CO_2 and land use history on the carbon dynamics of northern hardwood forests. *Global Change Biology*, *8*, 545–562. https://doi.org/10.1046/j.1365-2486.2002.00482.x

Parazoo, N. C., Coleman, R. W., Yadav, V., Stavros, E. N., Hulley, G., & Hutyra, L. (2021). Diverse biosphere influence on carbon and heat in mixed urban Mediterranean landscape revealed by high resolution thermal and optical remote sensing. *The Science of the Total Environment*, *806*, 151335. https://doi.org/10.1016/j.scitotenv.2021.151335

Park, C., Gerbig, C., Newman, S., Ahmadov, R., Feng, S., Gurney, K., et al. (2018). CO_2 transport, variability, and budget over the Southern California air basin using the high-resolution WRF-VPRM model during the CalNex 2010 campaign. *Journal of Applied Meteorology and Climatology*, *57*(6), 1337–1352. https://doi.org/10.1175/JAMC-D-17-0358.1

Parker, G. G. (2020). Tamm review: Leaf Area Index (LAI) is both a determinant and a consequence of important processes in vegetation canopies. *Forest Ecology and Management*, *477*, 118496. https://doi.org/10.1016/j.foreco.2020.118496

Pataki, D. E., Alig, R. J., Fung, A. S., Golubiewski, N. E., Kennedy, C. A., Mcpherson, E. G., et al. (2006). Urban ecosystems and the North American carbon cycle. *Global Change Biology*, *12*, 2092–2102. https://doi.org/10.1111/j.1365-2486.2006.01242.x

Pataki, D. E., Bowling, D. R., & Ehleringer, J. R. (2003). Seasonal cycle of carbon dioxide and its isotopic composition in an urban atmosphere: Anthropogenic and biogenic effects. *Journal of Geophysical Research*, *108*(D23). https://doi.org/10.1029/2003jd003865

Pataki, D. E., Carreiro, M. M., Cherrier, J., Grulke, N. E., Jennings, V., Pincetl, S., et al. (2011). Coupling biogeochemical cycles in urban environments: Ecosystem services, green solutions, and misconceptions. *Frontiers in Ecology and the Environment*, *9*, 27–36. https://doi.org/10.1890/090220

Pataki, D. E., Emmi, P. C., Forster, C. B., Mills, J. I., Pardyjak, E. R., Peterson, T. R., et al. (2009). An integrated approach to improving fossil fuel emissions scenarios with urban ecosystem studies. *Ecological Complexity*, *6*, 1–14. https://doi.org/10.1016/j.ecocom.2008.09.003

Piana, M. R., Aronson, M. F. J., Pickett, S. T. A., & Handel, S. N. (2019). Plants in the city: Understanding recruitment dynamics in urban landscapes. *Frontiers Ecology and Envrionment*, *17*(8), 455–463. https://doi.org/10.1002/fee.2098

Pickett, S. T. A., & Cadenasso, M. L. (2009). Altered resources, disturbance, and heterogeneity: A framework for comparing urban and non-urban soils. *Urban Ecosystems*, *12*, 23–44. https://doi.org/10.1007/s11252-008-0047-x

Rahman, M. A., Smith, J. G., Stringer, P., & Ennos, A. R. (2011). Effect of rooting conditions on the growth and cooling ability of *Pyrus calleryana*. *Urban Forestry and Urban Greening*, *10*, 185–192. https://doi.org/10.1016/j.ufug.2011.05.003

Randrup, T. B., McPherson, E. G., & Costello, L. R. (2001). Tree root intrusion in sewer systems: Review of extent and costs. *Journal of Infrastructure Systems*, *7*, 26–31. https://doi.org/10.1061/(asce)1076-0342(2001)7:1(26)

Rao, P., Hutyra, L. R., Raciti, S. M., & Templer, P. H. (2014). Atmospheric nitrogen inputs and losses along an urbanization gradient from Boston to Harvard Forest, MA. *Biogeochemistry*, *121*, 229–245. https://doi.org/10.1007/s10533-013-9861-1

R Core Team. (2020). *R: A language and environment for statistical computing*. R Foundation for Statistical Computing. Retrieved from https://www.R-project.org/

Reinmann, A., & Hutyra, L. R. (2017). Edge effects enhance carbon uptake and its vulnerability to climate change in temperate broadleaf forests. *Proceedings of the National Academy of Sciences of the United States of America*, *114*, 107–112. https://doi.org/10.1073/pnas.1612369114

Reinmann, A., Smith, I. A., Thompson, J. R., & Hutyra, L. R. (2020). Urbanization and fragmentation mediate temperate forest carbon cycle response to climate. *Environmental Research Letters*, *15*, 114036. https://doi.org/10.1088/1748-9326/abbf16

Rey, A., Pegorano, E., Tedeschi, V., De Parri, I., Jarvis, P. G., & Velentinit, R. (2002). Annual variation in soil respiration and its components in a coppice oak forest in Central Italy. *Global Change Biology*, *8*(9), 851–866. https://doi.org/10.1046/j.1365-2486.2002.00521.x

Richardson, A. D., Anderson, R. S., Arain, M. A., Barr, A. G., Bohrer, G., Chen, G., et al. (2012). Terrestrial biosphere models need better representation of vegetation phenology: Results from the North American carbon program site synthesis. *Global Change Biology*, *18*(2), 566–584. https://doi.org/10.1111/j.1365-2486.2011.02562.x

Richardson, A. D., Hufkens, K., Milliman, T., Aubrecht, D. M., Chen, M., Gray, J. M., et al. (2018). Data descriptor: Tracking vegetation phenology across diverse North American biomes using PhenoCam imagery. *Scientific Data*, *5*, 180028. https://doi.org/10.1038/sdata.2018.28

Roest, G. S., Gurney, K. R., Miller, S. M., & Liang, J. (2020). Informing urban climate planning with high resolution data: The Hestia fossil fuel CO_2 emissions for Baltimore, Maryland. *Carbon Balance and Management*, *15*(1), 22. https://doi.org/10.1186/s13021-020-00157-0

Roman, L. A., & Scatena, F. N. (2011). Street tree survival rates: Meta-analysis of previous studies and application to a field survey in Philadelphia, PA, USA. *Urban Forestry and Urban Greening*, *10*, 269–274. https://doi.org/10.1016/j.ufug.2011.05.008

Rosenzweig, C., Solecki, W., Hammer, S. A., & Mehrotra, S. (2010). Cities lead the way in climate-change action. *Nature*, *467*, 909–911. https://doi.org/10.1038/467909a

Rutberg, A. T., & Naugle, R. E. (2008). Population-level effects of immunocontraception in white-tailed deer (*Odocoileus virginianus*). *Wildlife Research*, *35*, 494–501. https://doi.org/10.1071/wr07128

Sargent, M., Barrera, Y., Nehrkorn, T., Hutyra, L. R., Gately, C. K., Jones, T. S., et al. (2018). Anthropogenic and biogenic CO_2 fluxes in the Boston urban region. *Proceedings of the National Academy of Sciences of the United States of America*. https://doi.org/10.1073/pnas.1803715115

Savage, K. B., & Davidson, E. A. (2001). Interannual variation of soil respiration in two New England forests. *Global Biogeochemical Cycles*, *15*(2), 337–350. https://doi.org/10.1029/1999GB001248

Schäfer, K. V. R., Oren, R., Ellsworth, D. S., Lai, C.-T., Herrick, J. D., Finzi, A. C., et al. (2003). Exposure to an enriched CO_2 atmosphere alters carbon assimilation and allocation in a pine forest ecosystem. *Global Change Biology*, *9*, 1378–1400.

Smith, I. A., Dearborn, V. K., & Hutyra, L. R. (2019). Live fast, die young: Accelerated growth, mortality, and turnover in street trees. *PLoS One*, *14*(5), e0215846. https://doi.org/10.1371/journal.pone.0215846

Smith, I. A., Hutyra, L. R., Reinmann, A. B., Thompson, J. R., & Allen, D. W. (2019). Evidence for edge enhancements of soil respiration in temperate forests. *Geophysical Research Letters*, *46*, 4278–4287. https://doi.org/10.1029/2019GL082459

Sprintsin, M., Chen, J. M., Desai, A., & Gough, C. M. (2012). Evaluation of leaf to canopy upscaling methodologies against carbon flux data in North America. *Biogeosciences*, *117*, G01023. https://doi.org/10.1029/2010jg001407

Stål, O¨ (1998). The interaction of tree roots and sewers: The Swedish experience. *Arboricultural Journal*, *22*, 359–367.

Stoval, A. E. I., Anderson-Teixeria, K. J., & Shugart, H. H. (2018). Assessing terrestrial laser scanning for developing non-destructive biomass allometry. *Forest Ecology and Management*, *427*, 217–229. https://doi.org/10.1016/j.foreco.2018.06.004

Stoy, P. C., Palmroth, S., Christopher Oishi, A., Siqueira, M. B. S., Juang, J., Novick, K., et al. (2005). Are ecosystem carbon inputs and outputs coupled at short time scales? A case study from adjacent pine and hardwood forests using impulse-response analysis. *Plant, Cell and Environment*, *30*, 700–710. https://doi.org/10.1111/j.1365-3040.2007.01655.x

Templer, P. H., Toll, J. W., Hutyra, L. R., & Raciti, S. M. (2015). Nitrogen and carbon export from urban areas through removal and export of litterfall. *Environmental Pollution*, *197*, 256e261. https://doi.org/10.1016/j.envpol.2014.11.016

Teskey, R., Wertin, T., Bauweraerts, I., Ameye, M., McGuire, M. A., & Steppe, K. (2014). Responses of tree species to heat waves and extreme heat events. *Plant, Cell and Environment*, *38*, 1699–1712. https://doi.org/10.1111/pce.12417

Townsend-Small, A., & Czimczik, C. I. (2010). Carbon sequestration and greenhouse gas emissions in urban turf. *Geophysical Research Letters*, *37*, L06707. https://doi.org/10.1029/2010GL042735

Trlica, A., Hutyra, L. R., Morreale, L. L., Smith, I. A., & Reinmann, A. B. (2020). Current and future biomass carbon uptake in Boston's urban forest. *The Science of the Total Environment*, *709*, 136196. https://doi.org/10.1016/j.scitotenv.2019.136196

Turnbull, J. C., Sweeney, C., Karion, A., Newberger, T., Lehman, S. J., Cambaliza, M. O., et al. (2015). Toward quantification and source sector identification of fossil fuel CO_2 emissions from an urban area: Results from the INFLUX experiment. *Journal of Geophysical Research: Atmospheres*, 292–312. https://doi.org/10.1002/2014JD022555.Received

United States Environmental Protection Agency. (2014a). *The 2011 National emissions inventory*. Retrieved from https://www.epa.gov/air-emissions-inventories/2011-national-emissions-inventory-nei-data

United States Environmental Protection Agency. (2014b). *Greenhouse gas reporting program*. Retrieved from https://www.epa.gov/ghgreporting

U.S. Energy Information Agency. (2013). *International Energy Outlook 2013* (Report No. DOE/EIA-0484(2013)).

Van Wagner, C. E. (1968). The line intersect method in forest fuel sampling. *Forest Science*, *14*(1), 20–27.

Vermote, E., Justice, C., Claverie, M., & Franch, B. (2016). Preliminary analysis of the performance of the Landsat 8/OLI land surface reflectance product. *Remote Sensing of Environment*. https://doi.org/10.1016/j.rse.2016.04.008

Wehr, R., Munger, J. W., McManus, J. B., Nelson, D. D., Zahniser, M. S., Davidson, E. A., et al. (2014). Seasonality of temperate forest photosynthesis and daytime respiration. *Nature*, *534*, 680–683. https://doi.org/10.1038/nature17966

Winbourne, J. B., Jones, T. S., Garvey, S. M., Harrison, J. L., Wang, L., Li, D., et al. (2020). Tree transpiration and urban temperatures: Current understanding, implications, and future research directions. *BioScience*, *70*(7), 576–588. https://doi.org/10.1093/biosci/biaa055

Yin, Y., Bowman, K., Bloom, A. A., & Worden, J. (2010). Detection of fossil fuel emissions trends in the presence of natural carbon cycle variability. *Environmental Research Letters*, *14*, 084050. https://doi.org/10.1088/1748-9326/ab2dd7

Zhang, L., Hu, Z., Fan, J., Zhou, D., & Tang, F. (2014). A meta-analysis of the canopy light extinction coefficient in terrestrial ecosystems. *Frontiers of Earth Science*, *8*(4), 599–609. https://doi.org/10.1007/s11707-014-0446-7

Zhang, X., Friedl, M., Schaaf, C. B., Strahler, A. H., & Schneider, A. (2004). The footprint of urban climates on vegetation phenology. *Geophysical Research Letters*, *31*(12). https://doi.org/10.1029/2004GL020137

Zhao, M., Kong, Z. H., Escobedo, F. J., & Gao, J. (2010). Impacts of urban forests on offsetting carbon emissions from industrial energy use in Hangzhou, China. *Journal of Environmental Management*, *91*, 807–813. https://doi.org/10.1016/j.jenvman.2009.10.010

Zhao, S., Liu, S., & Zhou, D. (2016). Prevalent vegetation growth enhancement in urban environment. *Proceedings of the National Academy of Sciences of the United States of America*. https://doi.org/10.1073/pnas.1602312113

Zhao, T. T., Brown, D. G., Fang, H. L., Theobald, D. M., Liu, T., & Zhang, T. (2012). Vegetation productivity consequences of human settlement growth in the eastern United States. *Landscape Ecology*, *27*, 1149–1165. https://doi.org/10.1007/s10980-012-9766-8

Zhou, W., Fisher, B., & Pickett, S. T. (2019). Cities are hungry for actionable ecological knowledge. *Frontiers in Ecology and the Environment*, *17*, 135. https://doi.org/10.1002/fee.2021